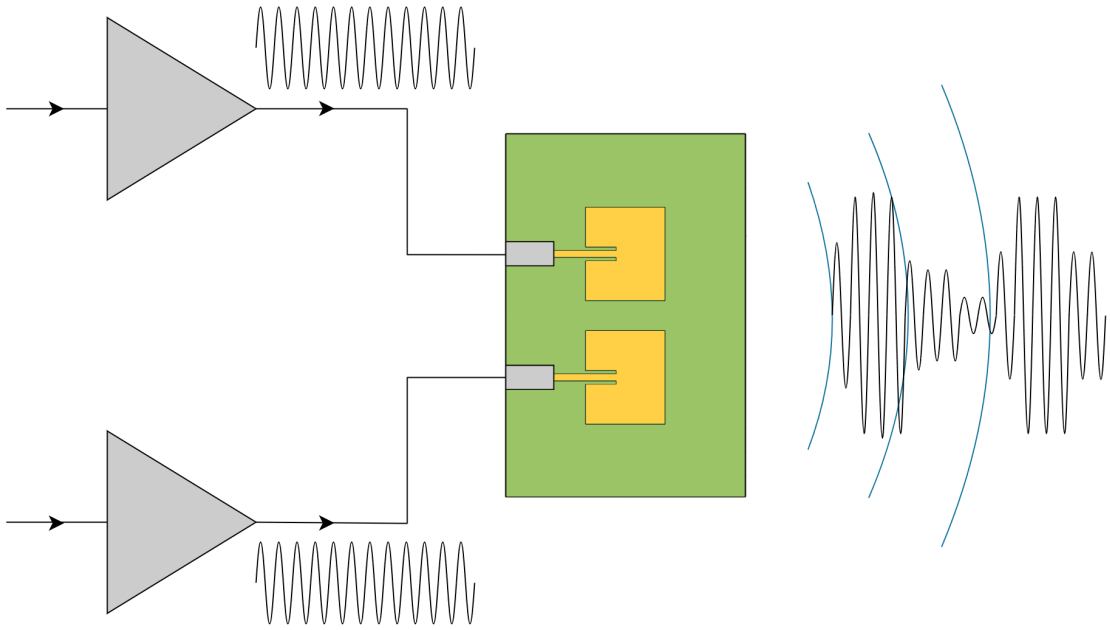

FPGA-controlled Outphasing Modulator Using A Power Combining Antenna

Bachelor degree project report in Electrical Engineering

Jakob Gunnarsson, Christopher Ek & Simon Westergren

Group: EENX16-VT25-0033

DEPARTMENT OF ELECTRICAL ENGINEERING
CHALMERS UNIVERSITY OF TECHNOLOGY
Gothenburg, Sweden 2025
www.chalmers.se

Bachelor degree project report 2025

FPGA-controlled Outphasing Modulator Using A Power Combining Antenna

Jakob Gunnarsson, Christopher Ek & Simon Westergren

Department of Electrical Engineering
Chalmers University of Technology
Gothenburg, Sweden 2025

FPGA-controlled Outphasing Modulator Using A Power Combining Antenna
Jakob Gunnarsson, Christopher Ek & Simon Westergren

© Jakob Gunnarsson, Christopher Ek & Simon Westergren, 2025.

Supervisors: Rob Maaskant & Iaroslav Shilinkov, Department of Electrical Engineering
Examiner: Erik Ström, Department of Electrical Engineering

Bachelor degree project report 2025
Department of Electrical Engineering
Chalmers University of Technology
SE-412 96 Gothenburg
Sweden
Telephone +46 31 772 1000

Cover: Illustration of an outphasing system with a two-element patch antenna array as the power combiner, where the phase modulated inputs generate an amplitude modulated output.

Typeset in LaTeX
Gothenburg, Sweden 2025

FPGA-controlled Outphasing Modulator Using A Power Combining Antenna

Jakob Gunnarsson, Christopher Ek & Simon Westergren
Department of Electrical Engineering
Chalmers University of Technology

Abstract

Coupling between antenna elements is often an undesired characteristic in antenna arrays, due to its distortion of radiation patterns and degradation of beamforming accuracy. However, if this coupling could be exploited in outphasing through load modulation, it has the potential to improve total system efficiency. This project aimed to design a high-efficiency outphasing system for communication applications, consisting of two power amplifiers (PAs) and a power combining antenna array.

To evaluate how different load impedances affect PA performance, a custom active vector-receiver load-pull setup was constructed and calibrated using an FPGA board. This setup enabled precise control over the presented load impedance to the PAs and was critical for measuring power added efficiency and output power under dynamic loading conditions. The resulting load-pull data informed the selection of ideal 2-port S-parameters for the power combiner. Based on these, a two-element patch antenna array was designed to serve as the combiner. Separate matching networks were implemented to match the antenna ports to the desired S-parameters. Two types of matching networks were considered: using lumped components and using microstrip lines. Using lumped components, the desired S-parameters were able to be matched quite well, yielding an error of around 9% whereas the microstrip line network was unable to provide sufficient matching in its current configuration.

Using the PA load-pull data and the S-parameters of the designed antenna, the performance of the outphasing system was tested through simulations in both MATLAB and CST. The results confirmed that outphasing was achievable with this setup, where amplitude modulation was realized by steering the antenna beam away from the receiver. Additionally, the simulations indicated that implementing an appropriate matching network could enhance the overall system efficiency.

Keywords: antenna, load modulation, antenna array, outphasing, power amplifiers, load-pull, FPGA, matching network.

Sammanfattning

Koppling mellan antennelement är ofta en oönskad egenskap i gruppantenner, då den kan orsaka distorsion i strålningsmönster och försämra precisionen i beamforming. Om denna koppling istället kan utnyttjas i outphasing genom lastmodulering, kan systemets verkningsgrad potentiellt förbättras. Syftet med projektet var att konstruera ett outphasingsystem med hög verkningsgrad för kommunikationsapplikationer, bestående av två effektförstärkare och en gruppantenn som används som effektkombinator.

För att utvärdera hur olika lastimpedanser påverkar förstärkarnas prestanda, konstruerades och kalibrerades en egenutvecklad aktiv vektor-mottagare för load-pull mätningar med hjälp av ett FPGA-kort. Denna uppställning möjliggjorde noggrann styrning av den presenterade lastimpedansen till effektförstärkarna och var avgörande för mätning av både *power added efficiency* och uteffekt under dynamiska belastningsförhållanden. Den uppmätta load-pull-datan låg till grund för valet av optimala tvåports S-parametrar för effektkombinatorn. Utifrån detta designades en gruppantenn bestående av patchantenner för att fungera som kombinator. Separata matchningsnätverk implementerades för att matcha antennportarna till de önskade S-parametrarna. Två typer av matchningsnätverk utvärderades: ett baserat på diskreta komponenter och ett baserat på mikrostripledare. Med diskreta komponenter kunde de önskade S-parametrarna uppnås med en felmarginal på cirka 9 %, medan nätverket bestående av mikrostripledare inte lyckades uppnå den önskade matchningen i sin nuvarande uppsättning.

Med hjälp av förstärkarnas load-pull-data och de uppmätta S-parametrarna för den designade antennen, testades outphasing-systemets prestanda genom simuleringar i både MATLAB och CST. Resultaten bekräftade att outphasing kunde uppnås med denna uppsättning, där amplitudmodulering realiserades genom att styra antennens lob bort från mottagarantennen. Simuleringarna visade dessutom att implementeringen av ett lämpligt matchningsnätverk skulle förbättra systemets totala verkningsgrad ytterligare.

Acknowledgements

We would like to extend our sincere thanks to Dr. Gregor Lasser for his expertise and the numerous discussions regarding the characterization of the power amplifiers. Furthermore, we would like to thank our supervisors Dr. Rob Maaskant and Iaroslav Shilinkov. Their consistent availability, constructive feedback, and timely responses to questions were deeply appreciated and were essential for the progress of the project.

Jakob Gunnarsson, Christopher Ek and Simon Westergren, Gothenburg, May 2025

List of Acronyms

Below is the list of acronyms that have been used throughout this thesis listed in alphabetical order:

ADC	Analog-to-Digital Converter
ASK	Amplitude Shift Keying
DAC	Digital-to-Analog Converter
DC	Direct Current
DUT	Device Under Test
FPGA	Field-Programmable Gate Array
FSK	Frequency Shift Keying
PA	Power Amplifier
PAE	Power Added Efficiency
PSK	Phase Shift Keying
PWM	Pulse Width Modulation
QAM	Quadrature Amplitude Modulation
RF	Radio Frequency
SOL	Short Open Load
SOLT	Short Open Load Through
VNA	Vector Network Analyzer

Nomenclature

Below is the nomenclature of indices, parameters, and variables that have been used throughout this thesis.

Indices

i, j	Port indices used in the S-parameter matrix (input/output ports)

Parameters

Z_0	Characteristic impedance, typically 50 Ω
λ_0	Free space wavelength
A_0	Constant amplitude of the decomposed outphasing signals
S_{ij}	S-parameter from port j to i
$\Delta\theta$	Difference in outphasing angle between intersections of outphasing circles
L	Length of the patch antenna
W	Width of the patch antenna
x_0	Distance between feed point and center of the first patch antenna
x_1	Distance between feed point and center of the second patch antenna
dx	Distance between antenna elements
ε_{r}	Dielectric material of antenna substrate
h	Height of dielectric substrate
t	Thickness of metal patch
L_1, L_2	Lumped component inductance in matching network at ports 1 and 2
C_1, C_2	Lumped component capacitance in matching network at ports 1 and 2

Variables

a_1, a_2, a_3	Forward traveling waves into port 1, 2 and 3
b_1, b_2, b_3	Reflected or outgoing waves at ports 1, 2, and 3
P_{in}	Input power
P_{out}	Output power
P_{DC}	Consumed DC power
PAE	Power Added Efficiency
Γ	Reflection coefficient
Γ_{in}	Input reflection coefficient
Γ_{L}	Load reflection coefficient
Γ_{PA_1}, Γ_{PA_2}	Load reflection coefficient seen by PA 1 and 2 in outphasing
Z_{L}	Load impedance
$S(t)$	Original signal to be transmitted
$S_1(t)$, $S_2(t)$	Constant envelope signals created from $S(t)$
θ	Outphasing angle

Contents

List of Acronyms **ix**

Nomenclature **xi**

List of Figures **xiv**

List of Tables **xvi**

1 Introduction **3**
1.1 Background . . . 3
1.2 Purpose . . . 4
1.3 Problem . . . 4
1.4 Scope . . . 4

2 Theory **7**
2.1 Power Amplifiers . . . 7
2.2 Digital Modulation . . . 9
2.3 Load-pull PA Characterization . . . 10
2.4 Outphasing . . . 13
2.4.1 Load Modulation . . . 14
2.4.2 Combiner Design . . . 17
2.4.3 Power Combining Antennas . . . 18
2.5 Patch Antennas . . . 18
2.5.1 Microstrip Line . . . 19
2.5.2 Antenna Array . . . 20
2.5.3 Impedance Matching . . . 20
2.5.4 Gain and Friis' Equation . . . 21

3 Methods **23**
3.1 Load-Pull Setup . . . 23
3.1.1 Generating Impedances And Measuring DUT . . . 25
3.1.2 Calibration . . . 25
3.1.3 Parameter Calculations . . . 26
3.1.4 Measurement Region Adjustments . . . 27
3.2 Analytical Combiner S-parameter Calculations . . . 27
3.3 Antenna Design . . . 30
3.3.1 Matching Network . . . 31

3.3.2 Exploratory Designs 32
3.4 Outphasing Simulations 32
3.4.1 Analytical S-parameter Simulations 33
3.4.2 Antenna Combiner Simulations 34

4 Results **35**
4.1 Load-Pull 35
4.2 Optimal Combiner S-parameters 36
4.3 Antenna Design 37
4.3.1 Lumped Component Matching Network 39
4.3.2 Microstrip Line Matching Network 40
4.4 Outphasing Simulations 41
4.4.1 Resulting Load Modulation on the PAs 41
4.4.2 Radiation Patterns at Outphasing 42
4.4.3 Total Power and PAE 44

5 Discussion **47**
5.1 Power Amplifiers 47
5.2 Load-Pull Setup 47
5.3 Antenna Design 48
5.4 Outphasing Simulations 49

6 Conclusion **51**

A Appendix **I**
A.1 Exploratory Designs I
A.2 CST Outphasing Simulation Data II

List of Figures

2.1 The 1 dB compression point illustrated where the actual output power of the PA diverges from the linear approximation by 1 dB. 7
2.2 Diagram of how different PA classes operate in relation to the transistor cutoff voltage (right). Transistor showing the gate-source voltage V_{GS}, drain-source voltage V_{DS}, and drain current I_{DS} (left). The waveforms shown here are the input signals, where some classes operate with parts of the signal wave in cutoff. 8
2.3 Simplified schematic of a power amplifier as the DUT in a traditional passive load-pull setup. 10
2.4 Simplified schematic of a power amplifier as the DUT in a passive vector-receiver load-pull setup. 11
2.5 Simplified schematic of a power amplifier as the DUT in an active vector-receiver load-pull setup. 12
2.6 Synthesized examples of how load-pull contour plots can look for arbitrary parameters 1 and 2 (output power or PAE for example). . . 12
2.7 Block diagram of the outphasing process 13
2.8 Complex vector representation of signal decomposition with differential phase shift θ. 14
2.9 Schematics of a general 3-port circuit-based power combiner, where the two input ports (ports 1 and 2) combine in the output port (port 3). 15
2.10 Example of load modulation circle placement from [6], *Copyright © 2015 IEEE*. Reproduced with permission 17
2.11 Power combining antenna array configuration where the original signal is reproduced in free space. 18
2.12 Schematic of a patch antenna, showing both a top-down view (left) and a cross-section (right). 19

3.1 Picture of the load-pull setup in the lab with labeled components and instruments. 23
3.2 The load-pull setup schematic, illustrating the uncalibrated measured waves denoted with sub-index m which correspond to the incoming and reflected waves at the ports of the DUT. 24
3.3 The antenna design schematic showing the dimension parameters for patch element i. 30

3.4 Schematic of the lumped components matching network for antenna element i. 31
3.5 Schematic of the microstrip line matching network for antenna element i. 32

4.1 Load-pull results illustrating how the parameters PAE and P_{out} change depending on the load impedance presented to the PA, with an average input power of 3.93 dBm. 35
4.2 Analytical outphasing load modulation circles overlaid on PAE and P_{out} contours. The figure illustrates the placement of the circles relative to the PA characteristics. The dots mark the point corresponding to $\theta = 0°$, and as θ increases, the load impedances trace the circles in the direction of the arrows. 36
4.3 Normalized Power added efficiency vs. back-off power level for the 4 different picks of S-parameters where $0° < \theta < 90°$. 37
4.4 S-parameters and co-polar embedded element pattern for the antenna array without matching networks for the ports. 39
4.5 Predicted load modulation circles for the different antenna feeding configurations compared against the target design. The dots indicate the point of maximum system output power. As θ increases, the load on the PAs traject along the circles in the direction of the arrows. . . 41
4.6 Output waves of the PAs at different outphasing angles which corresponds to the magnitude of the input waves of the antenna combiner, $|a_{1,\text{comb}}|$ and $|a_{2,\text{comb}}|$. 42
4.7 Total radiation patterns (φ constant) for the antenna with the lumped component matching network for the lowest, intermediate, and maximum gain in broadside. 43
4.8 Total radiation patterns (φ constant) for the antenna with the microstrip line matching network for the lowest, intermediate, and maximum gain in broadside. 43
4.9 IEEE Gain of the antennas at broadside as a function of the outphasing angle θ. 44
4.10 Normalized received power at broadside against the outphasing angle θ. 44
4.11 Normalized total PAE versus back-off power level in dB for $0° < \theta < 180°$. As θ increases, the plots trace the curve in the direction indicated by the arrows. 45

A.1 Schematic of single patch antenna with two orthogonally polarized feed-lines. II

List of Tables

4.1 S-parameters for the selected combiner design in rectangular and polar form. 37
4.2 Dimensions for the patch antenna elements without matching network. 38
4.3 Values for the lumped component matching networks at ports 1 and 2. 39
4.4 S-parameters of the antenna with lumped component matching network in rectangular and polar form. 40
4.5 Dimensions of the microstrip line matching networks at ports 1 and 2. 40
4.6 S-parameters of the antenna with microstrip matching network in rectangular and polar form. 40

A.1 CST outphasing simulation results using lumped component matching network. II
A.2 CST outphasing simulation results using microstrip matching network. III

1
Introduction

1.1 Background

As the evolution of wireless connectivity continues to advance, the demand for higher data rates and more bandwidth increases. When designing these highly efficient communication systems, reducing the total power consumption becomes a crucial factor. This comes with the need for more efficient systems and improved power amplification techniques [1]. The approach explored in this project is by integrating nonlinear, highly efficient power amplifiers (PAs) using a technique known as outphasing [2]. This technique enables more efficient power utilization during amplitude modulation, particularly for high-order modulation schemes such as Quadrature Amplitude Modulation (QAM) [3].

The outphasing technique, first introduced by Chirex in 1935, involves generating two constant amplitude signals with a differential phase shift, θ [4]. These constant amplitude signals are then amplified separately using two highly efficient, nonlinear PAs. Finally, the two signals are combined using a power combiner, where the differential phase shift is translated into amplitude modulation of the output signal.

A crucial feature of outphasing is the use of a non-isolated power combiner, which introduces electrical coupling between its input ports. This coupling dynamically varies the load impedance seen by each PA as the differential phase shift between the two branches changes [5]. The nature of this modulation depends on the Scattering Parameters (S-parameters) of the combiner. The benefit of this is the fact that PA performance metrics, such as output power and power-added efficiency (PAE), are sensitive to load impedance. The coupling between the ports can thus be used to help modulate the amplitude of the signal. If utilized optimally, this effect, known as load modulation, can significantly improve the efficiency of the system, especially at power levels below the peak output, commonly referred to as power back-off.

To utilize load modulation effectively, the PA's performance dependence on load impedance must be characterized [6]. This is achieved through a technique called load-pull, in which the PA is systematically subjected to a range of load impedances while its performance is measured at each impedance [7]. These measurements allow for the prediction of the desired load modulation behavior, enabling the design of a power combiner that optimally leverages both load modulation and outphasing for maximized efficiency.

Traditionally, outphasing in wireless communication systems is implemented using a circuit-based power combiner before the signal is radiated by an antenna [3]. This however comes with the drawback of resistive losses in the combiner circuit. A possible work-around presented in more recent studies show that incorporating the power combiner into the antenna structure itself is a possibility. In this approach, the two signals recombine in free space, eliminating resistive losses in the combiner circuit. This integration, however, introduces new design considerations, particularly the role of mutual coupling between antenna elements in array configurations, which typically is an undesired effect, due to its distortion of radiation patterns and degradation of beamforming accuracy [8].

1.2 Purpose

This project explores a potential advantage of the inherent coupling between antenna array elements. Specifically, it investigates the use of a two-element antenna array as both a radiator and a power combiner in an outphasing architecture. In this configuration, the coupling between the elements may be exploited to achieve load modulation in free space, potentially improving efficiency of outphasing while also eliminating resistive losses associated with conventional circuit-combiners.

1.3 Problem

To fulfill the purpose, there were several problems that needed to be assessed. The main problems that are addressed in this project are the following:

- How can an active load-pull measurement setup be constructed and calibrated with the use of an FPGA board?
- By measuring the PAs with the load-pull setup, how does the Power Added Efficiency (PAE) and the output power depend on the load impedance?
- Using the results from the load-pull measurements, how should the antenna array be designed regarding input impedance and coupling to enable optimal outphasing performance?
- How can an outphasing system with an antenna array as the power combiner be designed to improve efficiency?

1.4 Scope

Due mainly to time constraints, the project was subject to a few limitations. Firstly, the designed power combining antenna was only simulated and not manufactured and measured. Therefore, the complete outphasing system performance was not

tested with physical measurements, but rather simulated in order to estimate the performance. The patch antenna was the only type of antenna investigated as a combiner for this system. When characterizing the PAs, they were assumed to be identical. Consequently, only one of the amplifiers was characterized. This assumption was made for simplicity when simulating the PA performance during the outphasing simulations.

2
Theory

In this chapter, relevant theory behind the main parts of the project is presented. This includes theory regarding the linearity and efficiency of power amplifiers, load-pull methods, outphasing, and patch antennas.

2.1 Power Amplifiers

In a transmitting RF communication system, the PA is mainly used to amplify the transmission signal to reach a large enough signal strength at the receiver [9]. For this application, two common but conflicting PA design goals are linearity and efficiency. The linearity of a PA can be described as how well the shape of an input waveform is preserved at the output. This is highly dependent on the region in which it operates. A common measurement for the linear operation capability of a PA is the 1 dB compression point [4]. This point indicates at which output power the PA no longer follows a linear relation to the input power. This is illustrated in Fig. 2.1.

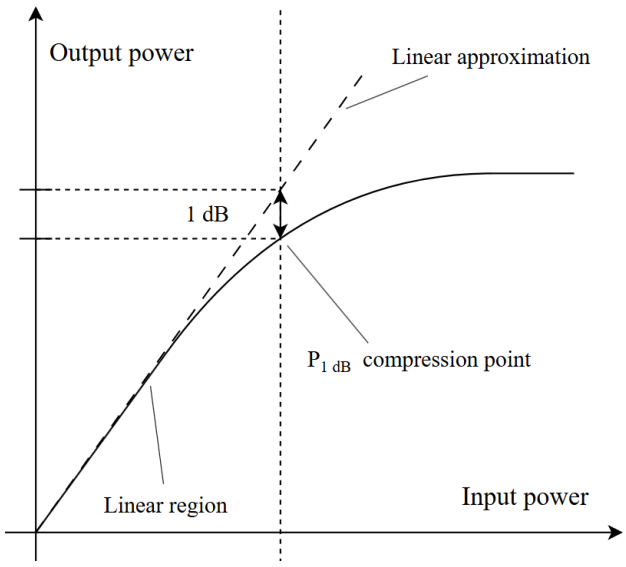

Figure 2.1: The 1 dB compression point illustrated where the actual output power of the PA diverges from the linear approximation by 1 dB.

Linear amplifiers are designed to be driven in the linear region, and the 1 dB compression point becomes the output limit for linear amplification. However, the lin-

earity of a PA is not only dependent on how it is driven with input but also on how it is designed.

It is common for the linearity of a PA to be categorized in classes such as class A, AB, B, C, D, and so on, where class A is the most linear but also the least efficient [10]. Fig. 2.2 illustrates how the classes are designed to operate compared to each other.

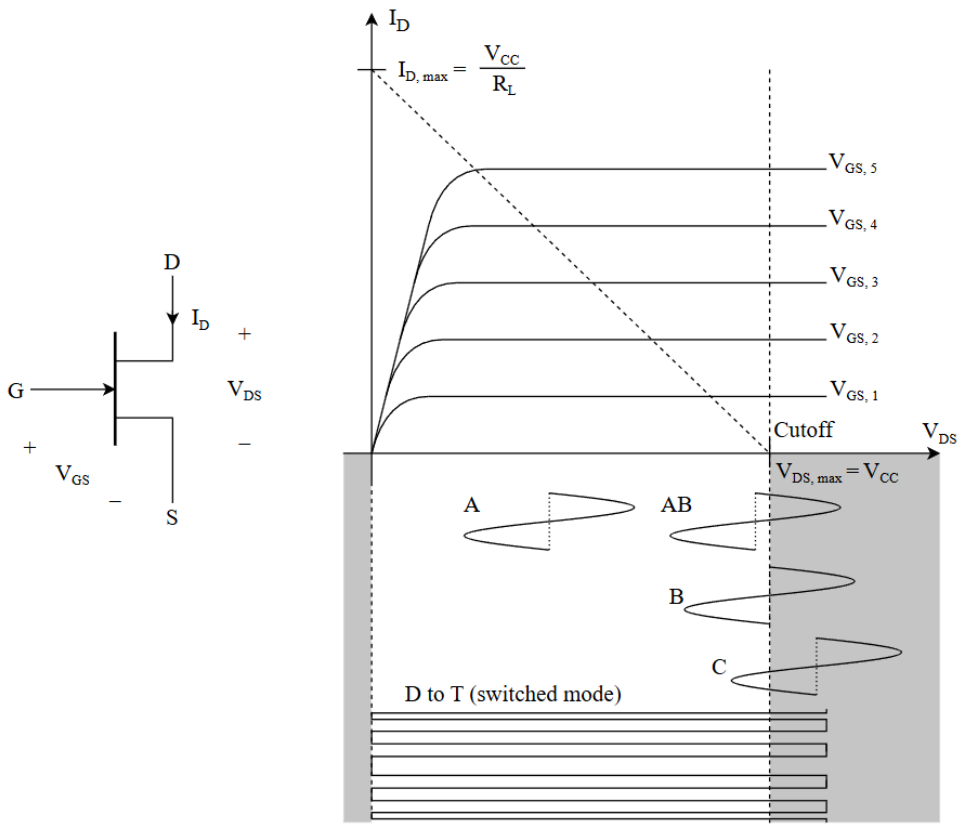

Figure 2.2: Diagram of how different PA classes operate in relation to the transistor cutoff voltage (right). Transistor showing the gate-source voltage V_{GS}, drain-source voltage V_{DS}, and drain current I_{DS} (left). The waveforms shown here are the input signals, where some classes operate with parts of the signal wave in cutoff.

The class A amplifier conducts throughout the 360 degrees of the input signal's wavelength [11]. This is done by applying a constant bias gate voltage to ensure the transistor operates in the linear region for a given input signal. This results in low distortion, but it also ensures that the transistor is always conducting drain current from the DC supply. Therefore, the class A amplifier consumes power even if there is no input signal, resulting in lower efficiency. The class A has a theoretical maximum efficiency of 50 %, but in practice it is typically around 40 to 45 % or lower [12]. Other classes can improve the efficiency by lowering or removing the bias voltage, but this creates problems with distortion and quality of the output signal.

Class B amplifiers, for example, do not have a bias DC voltage, and the transistors only conduct around 180 degrees of the signal wavelength [11]. By using two opposite-type transistors, both the negative and positive half-wavelengths can be amplified and combined at the output. However, this also creates some distortion around the zero voltage point of the output signal. This is due to the cutoff voltage on both transistors that cuts off the input at voltages near zero. The class AB amplifier counteracts this distortion by adding a small bias voltage, which results in a more linear amplifier with slightly lower efficiency than class B. In general, the trade-off when designing a linear amplifier is lower efficiency [10]. The same is true the other way around.

The most efficient amplifiers are categorized as switched-mode amplifiers and class D is one of these. Also referred to as class S for RF and microwave frequencies [10]. Here, the transistor is used as a switch, to switch "on" or "off" the output voltage. In class D and S, the switch is used to pulse width modulate (PWM) a desired output signal. A low-pass or "reconstruction" filter is placed at the output to smooth out the PWM signal into the modulated waveform. This way the transistors will only conduct current when a signal is being sent. And as seen in Fig. 2.2 when the input is switched "on", the drain current I_{D} is equal to $I_{\mathrm{D,\ max}}$ while the drain-source voltage is zero. And when the input is switched "off", I_{D} is equal to zero while $V_{\mathrm{DS}} = V_{\mathrm{DS,max}} = V_{\mathrm{CC}}$. Then, an ideal switched-mode amplifier would not pull current and voltage from the DC supply at the same time, resulting in no power consumption. Therefore, the theoretical efficiency of a perfect switched-mode amplifier is 100 % [4]. In reality, it will be lower due to non-instantaneous switching. Depending on the application, it can be desirable to use these highly efficient amplifiers despite the nonlinearity. For example, in linear systems that can utilize nonlinear components, such as an outphasing system.

2.2 Digital Modulation

In most telecommunication systems, such as 5G, WiFi, and fiber optics, digital data must be transmitted over physical channels. However, these channels are inherently analog. To enable the transmission of digital information, a digital modulation technique is employed to encode the discrete data into a continuous waveform that can propagate effectively through the medium [13]. This is done by producing a so-called carrier signal of a high frequency. The digital data is embedded into this carrier by dividing the signal into discrete elements called symbols. Each symbol corresponds to a specific configuration of the wave's properties, namely its amplitude, phase, or frequency.

Modulating these properties enables the creation of various digital modulation schemes, such as Amplitude Shift Keying (ASK), Frequency Shift Keying (FSK), and Phase Shift Keying (PSK). Among these, a particularly efficient and widely adopted technique is Quadrature Amplitude Modulation (QAM), which combines both amplitude and phase modulation [14]. This hybrid approach allows multiple bits to be transmitted per symbol, dramatically improving spectral efficiency and making QAM

especially valuable in high-data-rate communication systems where bandwidth is limited.

Due to the varying amplitudes of the signals, QAM schemes put some key requirements on the power amplifiers used in these systems. Most importantly, linearity is essential, as the information is encoded into the shape of the signal waveform. Non-linear amplification will distort the shape and, consequently, the transmitted information. Additionally, the power amplifiers need to operate below their peak output power. This condition, known as power back-off, often leads to reduced efficiency [10]. As a result, evaluating efficiency at power back-off becomes a crucial parameter when analyzing the performance of power amplifier systems designed for amplitude-modulated signals.

2.3 Load-pull PA Characterization

Load-pull is a method to characterize a nonlinear active device under test (DUT). Characterization in this context can be described as the mapping of DUT parameters for a variety of impedances at the ports of the DUT. Often used to characterize RF power amplifiers, the method can be used to model how a PA's performance changes depending on the impedance at the input or output [7]. This makes it possible to find the impedances that optimize the parameters of a PA, which can then be used to design matching networks for the transistor. Load-pull measurements are performed by measuring the parameters of the PA for many different source and output impedances. However, there are different ways to conduct these measurements.

Load-pull measurement setups can generally be categorized as either active or passive [15]. This refers to the way of generating impedances at the ports of the DUT, with either active or passive components. But there are also different methods to measure the DUT during load-pull. Two ways of measuring the DUT are referred to as traditional and vector-receiver [16]. A traditional passive load-pull of an amplifier is performed with passive impedance tuners at the input and output of the PA, as seen in Fig. 2.3. This method uses power sensors to measure the power at the impedance tuners. The measurements are then de-embedded from the components in the setup to get the power at the input and output of the DUT. The parameters input power P_{in} and output power P_{out} are then given from these results.

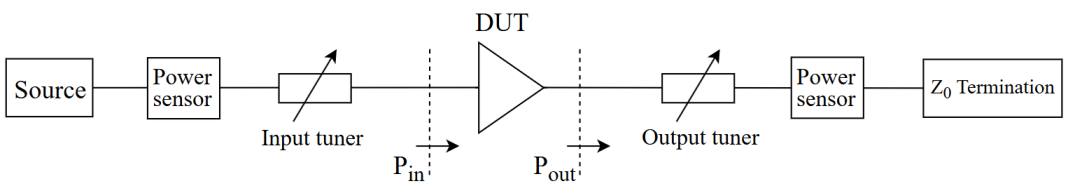

Figure 2.3: Simplified schematic of a power amplifier as the DUT in a traditional passive load-pull setup.

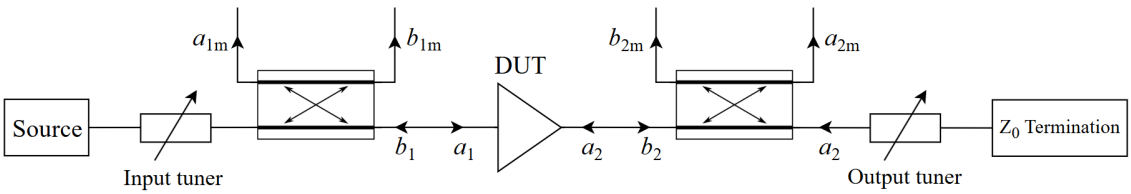

Figure 2.4: Simplified schematic of a power amplifier as the DUT in a passive vector-receiver load-pull setup.

Load-pull can also be performed by measuring the incoming and reflected power waves at the input and output. Measuring power waves in this way is referred to as vector-receiver load-pull, and it relies on low-loss bi-directional couplers connected to the DUT that allow measurements of the a and b waves, as seen in Fig. 2.4 [7], [16]. The variables a and b refer to power waves [17]. These measured waves can then be used to calculate the input impedance of the PA and the load impedance seen by the PA. Using the same notation for the waves as in Fig. 2.4, the input impedance is given by the reflection coefficient Γ_{in}

$$\Gamma_{\text{in}} = \frac{b_1}{a_1} \tag{2.1}$$

and the load impedance is given by the reflection coefficient Γ_{L}

$$\Gamma_{\text{L}} = \frac{a_2}{b_2}. \tag{2.2}$$

The corresponding impedance is then given by

$$Z = Z_0 \frac{1+\Gamma}{1-\Gamma} \tag{2.3}$$

where Z_0 is the characteristic impedance (50 Ω) and Γ is substituted for the corresponding reflection coefficient. Parameters of the DUT such as input and output power can also be derived from the measured waves [16]. Input power is

$$P_{\text{in}} = \frac{1}{2}\left(|a_1|^2 - |b_1|^2\right) \tag{2.4}$$

and output power is given by

$$P_{\text{out}} = \frac{1}{2}\left(|b_2|^2 - |a_2|^2\right). \tag{2.5}$$

To characterize the parameter PAE (Power Added Efficiency), the DC power consumed by the PA would also have to be measured during the load-pull. PAE is then given by

$$\text{PAE} = \frac{P_{\text{out}} - P_{\text{in}}}{P_{\text{DC}}} \tag{2.6}$$

where P_{DC} is the consumed DC power. These equations show that the load impedance is only dependent on the a and b waves measured in the setup. This makes it possible to create a load impedance by generating a reflected a_2 wave with a signal

generator, rather than letting the b_2 wave reflect off of the passive output tuner, as seen in Fig. 2.4. Generating a load impedance like this is referred to as active load-pull and is illustrated in Fig. 2.5 [15].

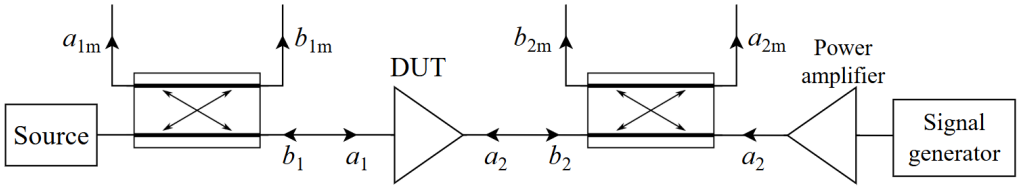

Figure 2.5: Simplified schematic of a power amplifier as the DUT in an active vector-receiver load-pull setup.

The generated signal a_2 in this setup can be specified digitally before being sent by the generator. And since the b_2 wave can be determined by the source signal, it is possible to generate any reflection coefficient using (2.2). Thereby generating any load impedance.

After load-pull measurements have been conducted, the collected parameter data is often visualized as a contour plot on the Smith chart. Each parameter data point can be associated with the load impedance that was presented to the DUT during the time of measurement. The measured load impedance can then be plotted on the Smith chart, and the value of the arbitrary parameter can be visualized with a contour plot. A fabricated example of such a plot, for an arbitrary DUT parameter, can be seen in Fig. 2.6.

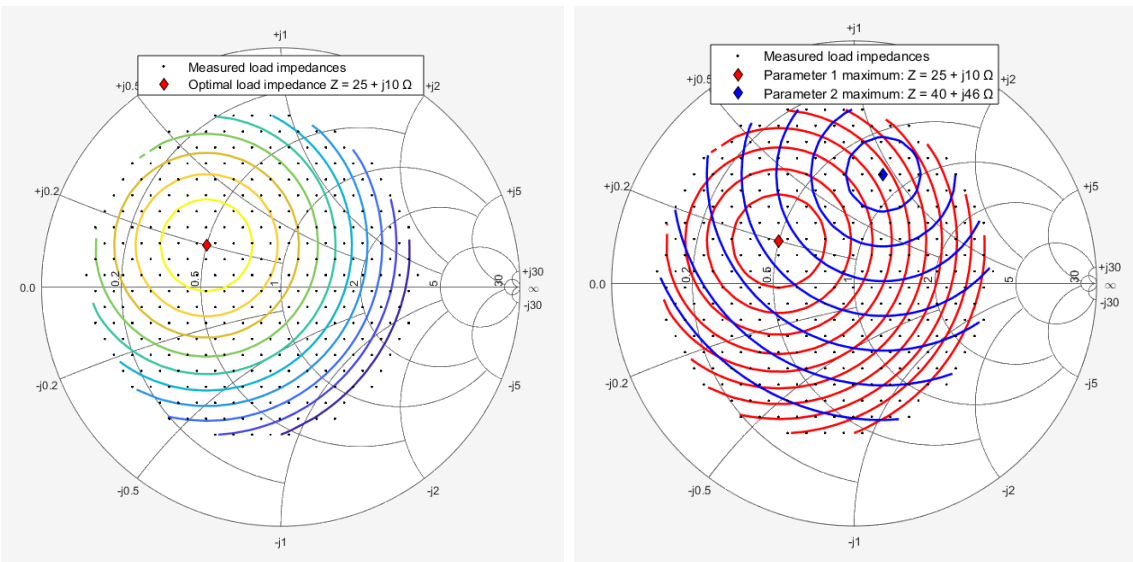

(a) Gradient contour with optimal load impedance marked for the parameter.

(b) Contour plots of two parameters with maximums marked.

Figure 2.6: Synthesized examples of how load-pull contour plots can look for arbitrary parameters 1 and 2 (output power or PAE for example).

The plots assist in analyzing how the parameters of the PA behave for different loads. The data collected can also be used to approximate the value of a parameter between points by interpolation, which provides an approximate mapping of the PA parameters. Thereby characterizing the PA in the region of the Smith chart where measurements were taken.

2.4 Outphasing

When maximizing efficiency in power amplifiers it comes with the drawback of non-linear amplification [10]. This makes them unfit for communication applications as linearity is essential to preserve the information in amplitude-modulated signals. One possible way to work around this is through a technique called outphasing. First introduced in 1935, the outphasing technique aims to utilize nonlinear, highly efficient PAs in linear power amplification systems [4, pp. 303–309], [18]. The aim of this is to improve efficiency and reduce the driving cost of RF power amplification systems. An outphasing system consists of two similar PAs that are driven in parallel at a fixed power level. The output of the two PAs are then added together through a power combiner to create the desired output signal. A simplified setup is presented in Fig. 2.7 below.

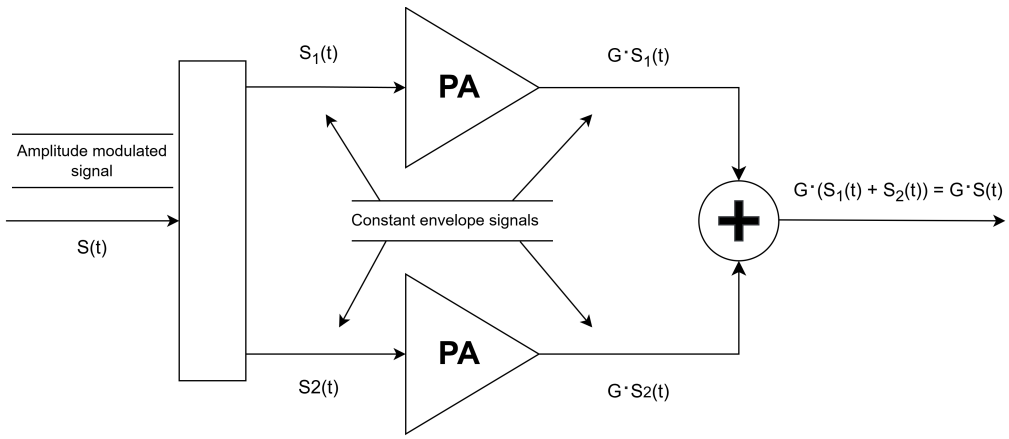

Figure 2.7: Block diagram of the outphasing process

In principle, the system works as follows: Suppose a phase and amplitude-modulated signal

$$S(t) = A(t) \cdot \cos(\omega t + \phi(t)) \tag{2.7}$$

is to be amplified. The idea of outphasing is then to convert the amplitude modulation $A(t)$ into a differential phase shift $\theta(t)$ between the two PA branches by creating two signals with constant amplitude $S_1(t)$ and $S_2(t)$ (also referred to as constant-envelope signals) such that $S_1(t) + S_2(t) = S(t)$ [18]. This would produce the sub-signals

$$\begin{aligned} S_1(t) &= A_0 \cdot cos[\omega t + \phi(t) + \theta(t)] \\ S_2(t) &= A_0 \cdot cos[\omega t + \phi(t) - \theta(t)], \end{aligned} \tag{2.8}$$

where

$$A(t) = 2A_0 \cos(\theta(t)) \implies \theta(t) = \cos^{-1}\left(\frac{A(t)}{2A_0}\right). \tag{2.9}$$

This process of decomposing the signal is depicted in the complex vector representation in Fig. 2.8. For simplicity, the phase modulation $\phi(t)$ is set to zero but can be any value and pass through the system unchanged.

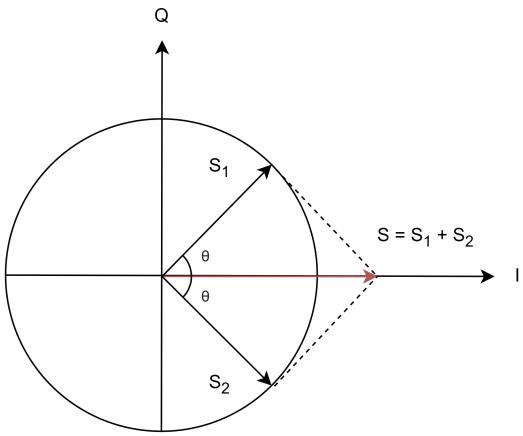

Figure 2.8: Complex vector representation of signal decomposition with differential phase shift θ.

$S_1(t)$ and $S_2(t)$ are then amplified separately by the two PAs. As the signals are of constant amplitude, they will be amplified without distortion despite the nonlinearity of the amplifiers. Thereafter $S_1(t)$ and $S_2(t)$ are added together at the output using a power combiner. Assume a perfectly isolated combiner, meaning the two input ports are electrically isolated and all the input power is transferred to the output port, is used. Also, let each PA have a voltage gain of G, the output signal is then theoretically given by

$$S_{\text{out}}(t) = G \cdot S_1(t) + G \cdot S_2(t) = G \cdot (S_1(t) + S_2(t)) = G \cdot S(t). \tag{2.10}$$

Thus, linearity is achieved [4, pp. 303–309].

Although this system presents almost perfect linearity and makes use of highly efficient PAs some further improvements can be made. When using a perfectly isolated combiner as assumed in Fig. 2.7 the PAs consume the same power regardless of the outphasing angle and system output power. This means a lot of power will be lost at lower system output amplitudes when two branches combine out of phase. To improve the efficiency, a non-isolated combiner is used instead [5], [18]. This introduces electrical coupling between the two PA branches resulting in a phenomenon known as load modulation.

2.4.1 Load Modulation

Load modulation is an important concept in designing outphasing PAs as it contributes significantly to improving the overall system efficiency [4, pp. 303–309]. The

principle relies on using a non-isolated power combiner that connects the two PA branches such that parts of the signal from the output of PA 1 will be transmitted to the output of PA 2. In other words, the PAs are essentially performing load-pull on each other. As the outphasing angle θ varies, the PAs will be presented with different impedances at their outputs, referred to as load impedances. When presented with larger load impedances, the output power of the PAs will decrease, since parts of the output wave reflect back from the load, as described by (2.2), (2.3) and (2.5). This enables amplitude modulation of the combined output signal by varying the load impedance of the PAs, hence the term Load Modulation.

An additional benefit of this is that high-efficiency PAs draw less DC supply power at higher loads. To take full advantage of this, the combiner should be designed such that the PAs are presented with higher load impedances as the outphasing angle increases. In this way, amplitude modulation is performed by varying the outphasing angle and presented load simultaneously, increasing the efficiency at power back-off. An important note is that load modulation introduces non-linearity into the outphasing system. However, with thorough analysis and characterization of the system through measurements, amplitude modulation can still be achieved in a controlled and predictable manner.

To achieve the desired load modulation action, the load seen by the PAs as θ varies, $\Gamma_{\mathrm{PA}_1}(\theta)$ and $\Gamma_{\mathrm{PA}_2}(\theta)$, can be predicted using the S-parameters of the combiner [6]. Consider a general 3-port circuit-based power combiner as illustrated in Fig. 2.9.

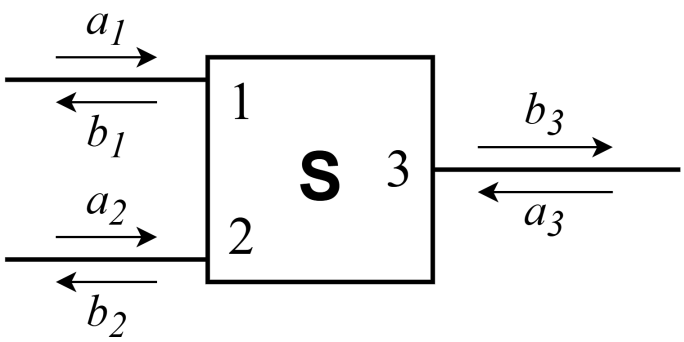

Figure 2.9: Schematics of a general 3-port circuit-based power combiner, where the two input ports (ports 1 and 2) combine in the output port (port 3).

Here, the outputs of the two PA branches are connected to ports 1 and 2 and the combined output signal is extracted from port 3. $\mathbf{S}$ is the 3×3 S-parameter matrix of the combiner, where [17]

$$S_{\mathrm{ij}} = \left.\frac{b_{\mathrm{i}}}{a_{\mathrm{j}}}\right|_{a_{i \neq j}=0} \qquad i, j \in \{1, 2, 3\}. \tag{2.11}$$

As a power combiner is a passive and reciprocal network, the S-matrix has certain constraints. Firstly, passivity means no power is added to the system by the combiner i.e.

$$\sum |a_{\mathrm{n}}|^2 \geq \sum |b_{\mathrm{n}}|^2, \tag{2.12}$$

which implies that the matrix $(\mathbf{I}) - (\mathbf{S})^H(\mathbf{S})$ is positive definite. Here, $(\mathbf{S})^H$ is the complex conjugate transpose of $\mathbf{S}$, and $\mathbf{I}$ is the identity matrix. Furthermore, reciprocity implies that

$$S_{mn} = S_{nm} \qquad m, n \in \{1, 2, 3\}. \tag{2.13}$$

Once the S-parameters of the combiner are known, the presented load on each PA can be predicted through a small signal analysis of the combiner [6]. The output waves of the PAs, which become the incident waves to the combiner, a_1 and a_2, are expressed in a similar matter as in (2.8). With complex representation, the following expressions are obtained

$$a_1 = A_1 e^{j\theta} \qquad a_2 = A_2 e^{-j\theta}. \tag{2.14}$$

Here, θ is the outphasing angle between the two branches, and A_1 and A_2 are the output amplitudes of each PA. Assuming there is no incident wave at the output port ($a_3 = 0$), the reflected b-waves at the inputs can be calculated according to

$$\begin{aligned} b_1 &= S_{11}a_1 + S_{12}a_2 \\ b_2 &= S_{21}a_1 + S_{22}a_2. \end{aligned} \tag{2.15}$$

Substituting (2.14) into (2.15) yields

$$\begin{aligned} b_1 &= S_{11}A_1e^{j\theta} + S_{12}A_2e^{-j\theta} \\ b_2 &= S_{22}A_2e^{-j\theta} + S_{21}A_1e^{j\theta}. \end{aligned} \tag{2.16}$$

The reflection coefficient at each input of the combiner, corresponding to the load seen at the output of PA is then calculated as

$$\begin{aligned} \Gamma_{\mathrm{PA}_1} &= \frac{b_1}{a_1} = S_{11} + \frac{A_2}{A_1}S_{12}e^{-j2\theta} \\ \Gamma_{\mathrm{PA}_2} &= \frac{b_2}{a_2} = S_{22} + \frac{A_1}{A_2}S_{21}e^{j2\theta}, \end{aligned} \tag{2.17}$$

which predicts the load modulation action on the PAs with respect to the outphasing angle θ. Going forward in this project, the amplitude A_1 and A_2 of the two branches are assumed to be equal and denoted as A. Thereby simplifying $\Gamma_{\mathrm{PA}_1}(\theta)$ and $\Gamma_{\mathrm{PA}_2}(\theta)$ as

$$\begin{aligned} \Gamma_{\mathrm{PA}_1}(\theta) &= S_{11} + S_{12}e^{-j2\theta} \\ \Gamma_{\mathrm{PA}_2}(\theta) &= S_{22} + S_{21}e^{j2\theta}. \end{aligned} \tag{2.18}$$

From this, it can be observed that when sweeping the outphasing angle θ, the reflection coefficients Γ_{PA_1} and Γ_{PA_2} will trace out circles on the Smith chart. These circles traject in opposite directions with origins in S_{11} and S_{22}. The 2θ factor in the exponent indicates that the presented load on the PAs will be periodic with a period of 180°. The coupling between the ports, S_{12} and S_{21} will determine the radius of the circles. As the combiner is a reciprocal network, $S_{12} = S_{21}$ as stated in (2.13), thus the circles have equal radii. Going forward, the circles given by (2.18) will be

referred to as Load Modulation Circles.

Furthermore, the output signal b_3 can also be predicted using the combiner S-parameters. Again, assuming that $a_3 = 0$ the output is given by

$$b_3 = S_{31}a_1 + S_{32}a_2. \tag{2.19}$$

Expanding a bit and substitutiong the a_1 and a_2 waves into 2.19 yields

$$b_3 = |S_{31}|\, e^{j\angle S_{31}} A e^{j\theta} + |S_{32}|\, e^{j\angle S_{32}} A e^{-j\theta}. \tag{2.20}$$

Consequently, the output signal will be dependent on both the phase and the amplitude of S_{31} and S_{32}

2.4.2 Combiner Design

Optimizing the outphasing system then ultimately comes down to designing a combiner with S-parameters that results in a desired load modulation action. At high powers, it is hard to predict the behavior of the PAs at different loads. Therefore, load-pull measurements are performed, which are then used to design the desired load modulation circles [6]. The goal of the combiner design is to have the circles intersect at the maximum PAE point at the same outphasing angle θ with output power decreasing as the outphasing angle increases. In addition to this, they should remain in the highest efficiency region possible. It is also desirable to have the same output power from both PAs, therefore the load modulation contours are to be balanced over the axis of output power symmetry. Fig. 2.10 presents an illustrative example of how this can look on the Smith chart for an outphasing system evaluated in [6].

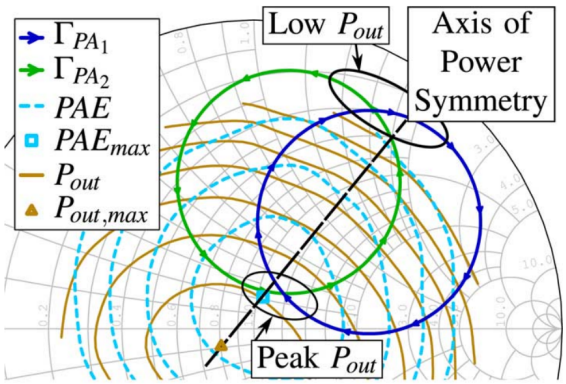

Figure 2.10: Example of load modulation circle placement from [6], *Copyright © 2015 IEEE*. Reproduced with permission

In traditional circuit-based combiners the physical design is based on connecting different lengths of series transmission lines and shunt reactances [18], [19]. The structure can then be tuned until the desired load modulation is achieved, using the small signal analysis from (2.18) to predict the load modulation.

2.4.3 Power Combining Antennas

The conventional way of using outphasing PAs is to connect them to a circuit-based power combiner as discussed above. The combined signal can then be radiated through an antenna at the output of the combiner [2]. However, using a circuit-based combiner comes with the drawback of resistive losses in the circuit. Instead, if the combining step is integrated into the antenna structure itself, the losses in the combiner circuit could be eliminated. The combining step is then instead performed in free space via superposition of the radiated electromagnetic waveforms. This approach thus has the potential to reduce resistive losses and improve the overall efficiency of the outphasing system.

The over-the-air power combining can be achieved by either using a radiator with two input ports [2], [3], or by using two (or more) single-port elements in an array configuration as is depicted in Fig. 2.11 [20].

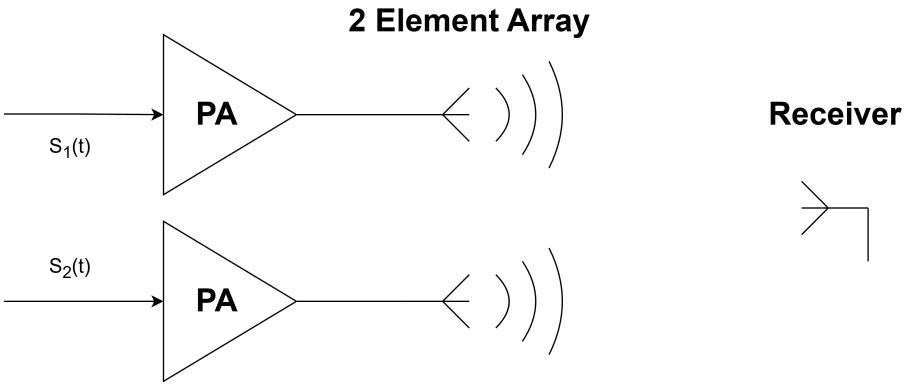

Figure 2.11: Power combining antenna array configuration where the original signal is reproduced in free space.

In this approach, the outputs of each PA branch are transmitted through individual antenna elements and the original phase- and amplitude modulated signal is reproduced via superposition at a certain angle in free-space.

2.5 Patch Antennas

In this project, a patch antenna array is used for power combining. The patch antenna is a low-profile narrow-band microstrip antenna. The antenna consists of a finite, very thin metal patch, with the thickness $t \ll \lambda_0$ (λ_0 being the free-space wavelength), placed above a ground plane with a thin dielectric substrate ε_r, with the height $h \ll \lambda_0$, separating the ground plane and the patch. In contrast to microstrip lines, the patch antenna benefits from a larger substrate thickness and lower dielectric constant since fringing fields are necessary for the patch to radiate [21]. Fig. 2.12 illustrates the dimensions of a patch antenna.

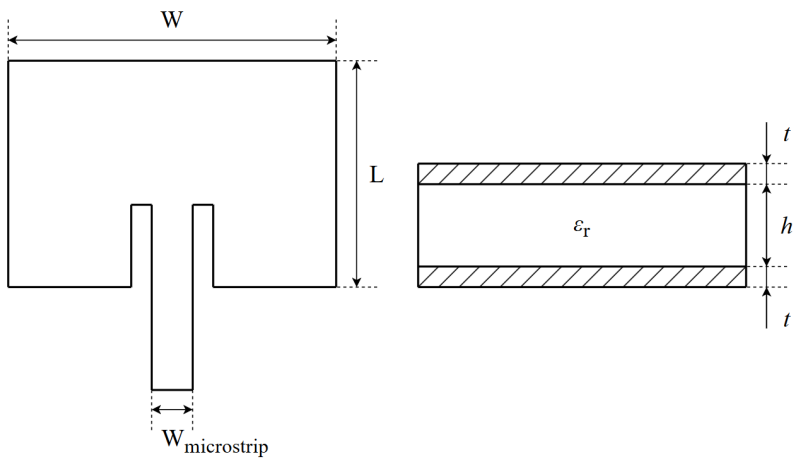

Figure 2.12: Schematic of a patch antenna, showing both a top-down view (left) and a cross-section (right).

The patch antenna becomes resonant when the length of the patch is approximately half the wavelength inside the substrate. The fringing fields will extend beyond the patch resulting in the electric length of the antenna being larger than the physical length. Therefore, the physical length is slightly shorter than half the wavelength [22]. To get an approximate value of the length, the following formula can be used

$$L \approx 0.49 \frac{\lambda_0}{\sqrt{\varepsilon_r}}. \tag{2.21}$$

More precise formulas are available in both [21], [22] but are not necessary since the length has to be tweaked to find the optimal performance for the project anyway. Therefore,(2.21) provides a sufficient initial length

The width is usually chosen to increase the bandwidth and simultaneously yield sufficient radiation efficiency. Usually, a trade-off has to be made between these two parameters. Furthermore, it will affect the dominant mode of the patch [22]. As an initial value for the width, the following equation is used

$$W = \frac{\lambda_0}{2} \sqrt{\frac{2}{\varepsilon_r + 1}}. \tag{2.22}$$

There are different methods to feed the patch antenna. The aperture-coupled feed has the benefit of enabling different thicknesses as well as dielectric constants of the dielectrics for the microstrip line and the patch antenna. The fringing fields for the microstrip lines can therefore be held small whilst being large for the antenna. Another common method to feed the patch antenna is a microstrip edge feed with an inset to the point yielding the necessary input impedance for matching to the wanted S_{11} coefficients [22].

2.5.1 Microstrip Line

Regardless of the matching method, a microstrip line has to be used. The microstrip line must be designed for a specified characteristic impedance Z_0. The design for-

mulas for the microstrip lines are the following [17]

$$\frac{W_{\text{microstrip}}}{h} = \begin{cases} \frac{8e^A}{e^{2A}-2}\ , \text{ for } W_{\text{microstrip}}/h < 2 \\ \frac{2}{\pi}\left\{B - 1 - \ln\left(2B-1\right) + \frac{\varepsilon_{\text{r}}-1}{2\varepsilon_{\text{r}}}\right\}\left(\ln(B-1) + 0.39 - \frac{0.61}{\varepsilon_{\text{r}}}\right)\ , \\ \qquad\qquad \text{for } W_{\text{microstrip}}/h > 2 \end{cases} \tag{2.23}$$

where

$$A = \frac{Z_0}{60}\sqrt{\frac{\varepsilon_{\text{r}}+1}{2}} + \frac{\varepsilon_{\text{r}}-1}{\varepsilon_{\text{r}}+1}\left(0.23 + \frac{0.11}{\varepsilon_{\text{r}}}\right) \tag{2.24}$$

and

$$B = \frac{377\pi}{2Z_0\sqrt{\varepsilon_{\text{r}}}}. \tag{2.25}$$

The characteristic impedance can be analytically verified using

$$Z_0 = \begin{cases} \frac{60}{\sqrt{\varepsilon_{\text{e}}}}\ln\left(\frac{8h}{W_{\text{microstrip}}} + \frac{W_{\text{microstrip}}}{4h}\right)\ , \text{ for } W_{\text{microstrip}}/h \leq 1 \\ \frac{120\pi}{\sqrt{\varepsilon_{\text{e}}}[W_{\text{microstrip}}/h + 1.393 + 0.667\ln\left(W_{\text{microstrip}}/h + 1.444\right)]}\ , \text{ for } W_{\text{microstrip}}/h > 1 \end{cases} \tag{2.26}$$

where the effective dielectric constant is found by

$$\varepsilon_{\text{e}} = \frac{\varepsilon_{\text{r}}+1}{2} + \frac{\varepsilon_{\text{r}}-1}{2}\frac{1}{\sqrt{1+12h/W_{\text{microstrip}}}}. \tag{2.27}$$

The length of the microstrip line will affect the phase of the wave and therefore the phase of the reflection coefficients.

2.5.2 Antenna Array

The antennas can be placed adjacent to one another with a distance dx between the elements. Since the antennas are in the reactive near-field, the antennas will be coupled which affects the input impedance. By changing the distance between the elements the coupling coefficients S_{ij} (where $i \neq j$) will change. Due to the distance dx between the elements, a small phase shift will occur between the two transmitted signals. This is due to the traveling distances of the signals not necessarily being the same due to the spatial difference; for a receiver placed between the two elements in broadside, the distance will be identical and no phase shift will occur [22].

2.5.3 Impedance Matching

The antennas should operate in the optimal region found from the load-pull. This is achieved by matching the S-parameters to the desired values. By changing the inset of the feed on the patch antenna, the input impedance can be slightly altered. If the necessary reflection coefficients for the port cannot be realized by only changing the inset feed, a matching network has to be designed. The simplest method of matching is using an L-network. This is done by connecting an inductance in series and a capacitance in parallel (or vice-versa) with the load. The matching network

also has to match the phase for the coupling coefficients which could complicate the matching of the reflection coefficients and alter the magnitude of the coupling. The necessary values for these can be found manually using the Smith chart or by simulations. Thereafter, the corresponding microstrip line can be calculated using Richard's Transformation [17].

2.5.4 Gain and Friis' Equation

The gain of an antenna is a measure that takes into account both the directional characteristics and the efficiency of an antenna. It is defined as the ratio of the radiation intensity for the antenna in a given direction to the isotropic power intensity [21]. The relative gain is calculated by

$$G_{\mathrm{IEEE}}(\theta, \varphi) = \frac{4\pi U(\theta, \varphi)}{P_{\mathrm{in}}} \tag{2.28}$$

where $U(\theta, \varphi)$ is the radiation intensity and P_{in} is the accepted input power. Commonly when the direction is not stated, the gain is taken for the maximum radiation point [21]. However, in this project, it will be taken as the gain in the broadside direction. The IEEE gain does not include reflection losses or polarization losses.

When two antennas are placed in direct Line-Of-Sight at a distance in the farfield region, the electromagnetic waves transmitted from an antenna are approximately a plane wave [21], [22]. The Friis Transmission Equation is used to find the received power from the transmitted power, for antennas in the farfield [21], and is found by

$$P_{\mathrm{r}} = \left(\frac{\lambda}{4\pi R}\right)^2 G_{\mathrm{t}} G_{\mathrm{r}} P_{\mathrm{in}}. \tag{2.29}$$

For an isotropic radiator, the gain is unity; approximating the receiver as an isotropic radiator then results in $G_{\mathrm{r}} = 1$. If the distance between the antennas is fixed and only one frequency is considered, the received power is proportional to

$$P_{\mathrm{r}} \propto G_{\mathrm{t}} P_{\mathrm{in}}. \tag{2.30}$$

This proportionality can be used to investigate the shape, and the relative value, of the received power for different outphasing angles.

3

Methods

This chapter presents the methods used throughout the project. The methods behind the load-pull measurements, analytical calculations of combiner S-parameters, antenna design, and outphasing simulations are described here.

3.1 Load-Pull Setup

To design a suitable antenna combiner for the two QPA9501 power amplifiers, they were characterized using an active vector-receiver load-pull setup. This is to determine what S-parameters the antenna combiner should present to the amplifiers for best performance in the outphasing system. The PAs were characterized for the parameters output power and PAE. The ZCU216 RFSoC FPGA board was used to generate and measure the signals in the setup. For this, the board's digital-to-analog converters (DACs) and analog-to-digital converters (ADCs) were used. Fig. 3.1 shows a labeled picture of the setup in the lab and Fig. 3.2 shows the schematic of the setup.

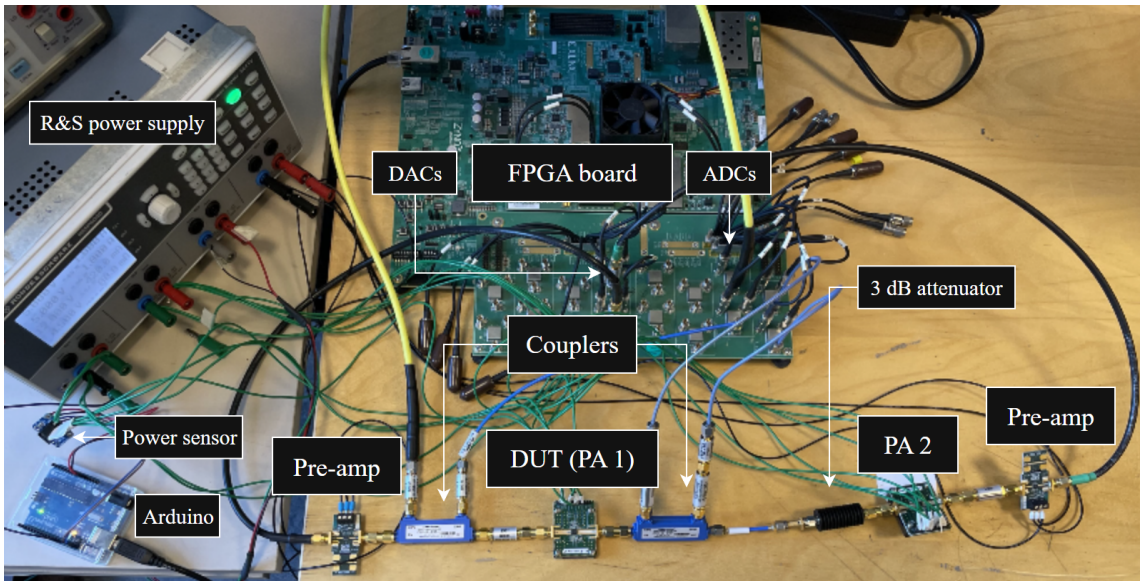

Figure 3.1: Picture of the load-pull setup in the lab with labeled components and instruments.

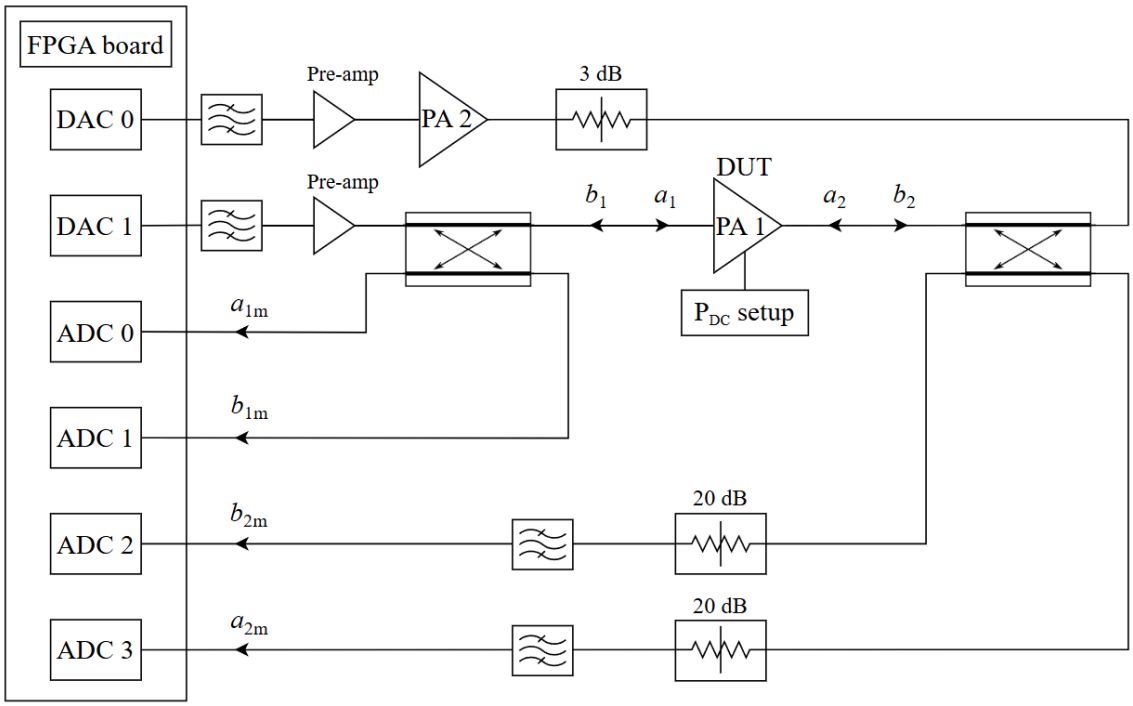

Figure 3.2: The load-pull setup schematic, illustrating the uncalibrated measured waves denoted with sub-index m which correspond to the incoming and reflected waves at the ports of the DUT.

The components used in the setup were filters, pre-amps, low-loss bi-directional couplers, and attenuators. The purpose of the filters, at the output of DAC 0 and 1, was to filter out harmonics from the DACs before reaching the pre-amps. The pre-amps then amplified the DAC signal to an appropriate power level of approximately 3.9 dBm for the input of the PAs. The output power of PA 2 was then reduced by 3 dB with the 3 dB attenuator before reaching PA 1. This was done to constrain the a_2 wave to always be lower in amplitude than the b_2 wave. Thereby constraining the load reflection coefficient to be lower than one. This was a safety precaution for the PAs since shorting the PAs could be damaging to them. Attenuators and filters were also used at ADC 2 and 3 to remove harmonics and reduce the large power levels generated by the PAs, avoiding damage to the ADCs. Finally, as this was a vector-receiver setup, it relied on the couplers at the input and output of the DUT to measure incoming and reflected waves separately. MATLAB was then used to conduct these measurements.

The board was controlled from MATLAB in order to control the signals from the DACs and save the measurements from the ADCs. The DC power consumption of the DUT was measured with an INA260 power sensor connected to an Arduino Uno. The DC measurements were then sent to MATLAB by the Arduino. In order to test the DUT for multiple load impedances, a script was written in MATLAB to generate different reflection coefficients.

3.1.1 Generating Impedances And Measuring DUT

The load impedance seen by the DUT was generated by fixing the input a_1 wave and changing the generated reflected a_2 wave. Then, by measuring the a_2 and b_2 waves, the reflection coefficient Γ_{L} is given by (2.2). The load impedance presented to the DUT could then be specified by changing the DAC 0 signal relative to the DAC 1 signal in Fig. 3.2.

To specify which impedances would be measured, a function was created to place a circle inside the Smith chart with a given radius and center. The function then placed evenly spaced points inside the circle, which corresponded to the impedances that would be generated. The points were then converted from Cartesian coordinates to amplitudes and phases, which then could be sent by DAC 0. This way, a chosen region of the Smith chart could be measured with a specified number of points. Each data point corresponded to a load impedance, and the saved data for a point were the measured waves $a_{1\mathrm{m}}$, $b_{1\mathrm{m}}$, $a_{2\mathrm{m}}$, $b_{2\mathrm{m}}$ and the consumed DC power. Calibration was then applied to this data before calculating the parameters output power and PAE.

3.1.2 Calibration

Before load-pull measurements were performed, the two ports of the setup were calibrated using an 8-term Short Open Load Through (SOLT) calibration, as presented in [23]. This method uses known short, open, load, and a standard through connection to conduct seven measurements, providing an 8-term error model for relative calibration. Later, a power sweep was performed to calibrate the absolute power measurements of the setup.

Firstly, the four calibration standards were measured with a calibrated Vector Network Analyzer (VNA). These measurements gave known values for the reflection coefficients of the short, open, and load standards, denoted as, Γ_{Short}, Γ_{Open} Γ_{Load} as well as the full 2×2 S-parameter matrix of the thru standard, $S_{ij,\mathrm{through}}$. The calibration of the load pull setup was then performed by first conducting a one-port Short Open Load (SOL) calibration on both ports separately, followed by a through calibration between the two ports.

The SOL calibration was done by first connecting the short to the first port, then sending a wave through that port and measuring the incoming and reflected wave with the ADCs. The uncalibrated measured reflection coefficient Γ_{mShort} was then calculated for the short. The subscript mS indicates that the reflection coefficient is an uncalibrated measurement of the short calibration standard. The same process was done for the open and load, giving Γ_{mOpen} and Γ_{mLoad}. Then, the error terms for the first port, β_1', γ_1' and δ_1', were calculated as follows

$$\begin{bmatrix} \beta_1' \\ \gamma_1' \\ \delta_1' \end{bmatrix} = \begin{bmatrix} -\Gamma_{\mathrm{mShort}} \cdot \Gamma_{\mathrm{Short}} & 1 & \Gamma_{\mathrm{mShort}} \\ -\Gamma_{\mathrm{mOpen}} \cdot \Gamma_{\mathrm{Open}} & 1 & \Gamma_{\mathrm{mOpen}} \\ -\Gamma_{\mathrm{mLoad}} \cdot \Gamma_{\mathrm{Load}} & 1 & \Gamma_{\mathrm{mLoad}} \end{bmatrix}^{-1} \begin{bmatrix} \Gamma_{\mathrm{Short}} \\ \Gamma_{\mathrm{Open}} \\ \Gamma_{\mathrm{Load}} \end{bmatrix}. \tag{3.1}$$

The same process was then repeated for the second port, giving the error terms β_2', γ_2' and δ_2'. The SOL calibration of the two ports gives six of the eight error terms needed for the full two-port calibration in [23]. The completely calibrated waves, a_i and b_i for port i are given by

$$\begin{bmatrix} a_\mathrm{i} \\ b_\mathrm{i} \end{bmatrix} = \alpha_\mathrm{i} \cdot \begin{bmatrix} 1 & \beta_\mathrm{i}' \\ \gamma_\mathrm{i}' & \delta_\mathrm{i}' \end{bmatrix} \begin{bmatrix} a_\mathrm{i\ m} \\ b_\mathrm{i\ m} \end{bmatrix} \tag{3.2}$$

where i can be substituted for 1 or 2, and α_i represents the last two error terms in the calibration. But by using only the six error terms, the waves can be partially calibrated using

$$\begin{bmatrix} \bar{a}_\mathrm{i} \\ \bar{b}_\mathrm{i} \end{bmatrix} = \begin{bmatrix} 1 & \beta_\mathrm{i}' \\ \gamma_\mathrm{i}' & \delta_\mathrm{i}' \end{bmatrix} \begin{bmatrix} a_\mathrm{i\ m} \\ b_\mathrm{i\ m} \end{bmatrix} \tag{3.3}$$

where $\bar{a}_\mathrm{i}$ and $\bar{b}_\mathrm{i}$ are the partially calibrated waves. These are related to the fully calibrated waves with

$$\begin{cases} a_\mathrm{i} = \alpha_\mathrm{i}\bar{a}_\mathrm{i} \\ b_\mathrm{i} = \alpha_\mathrm{i}\bar{b}_\mathrm{i}. \end{cases} \tag{3.4}$$

Then to calibrate the ports in relation to each other, the two ports were connected with the through standard. A signal was then sent from port 1, and all waves (a_1m, b_1m, a_2m and b_2m) were measured. The partially calibrated waves ($\bar{a}_1$, $\bar{b}_1$, $\bar{a}_2$ and $\bar{b}_2$) were then calculated from these measurements using (3.3). The error term α_2 could then be calculated with

$$\alpha_2 = (\bar{b}_2 - S_\mathrm{22,through}\bar{a}_2)^{-1}\bar{a}_1 S_\mathrm{21,through} \tag{3.5}$$

where $S_\mathrm{22,through}$ and $S_\mathrm{21,through}$ are the S-parameters of the through connector acquired from the VNA measurements. Since the calibration was a relative calibration, the error term $\alpha_1 = 1$.

To calibrate power measurements with the setup, a power sweep was performed. The power at port 1 was measured with a R&S NRP332N power sensor, for several different amplitudes sent by port 1. The difference in power, between the SOLT calibration of the waves and the power meter measurements, was assumed to be linear. Following this, the relation was modeled as a single coefficient that scaled the power measurements by the setup. By measuring the power with both the setup and the power meter at the same time, the constant coefficient ρ was calculated by dividing the two measurements. This constant was then applied when calculating the input power and output power.

3.1.3 Parameter Calculations

After the raw measured waves had been calibrated, they were used in the equations presented in Section 2.3. For every measured point, the load reflection coefficient was calculated with (2.2). When the input and output power were calculated, the constant power-calibration-coefficient ρ was multiplied to (2.4) and (2.5), which gives

$$P_{\text{in}} = \frac{1}{2}\left(|a_1|^2 - |b_1|^2\right)\rho \tag{3.6}$$

and

$$P_{\text{out}} = \frac{1}{2}\left(|b_2|^2 - |a_2|^2\right)\rho. \tag{3.7}$$

The P_{in} and P_{out} from these equations were then used in (2.6) to calculate PAE, where P_{DC} is the measured DC power for the data point. The calculated parameters for all reflection coefficients were then saved in MATLAB to be visualized as contour plots in the Smith chart. These plots were then used to decide how the load modulation circles should be placed, and in turn, determine the desired 2-port S-parameters of the antenna combiner.

3.1.4 Measurement Region Adjustments

After a load-pull measurement, it was observed that the measurement region in the Smith chart had been shifted in some direction from the region specified in the MATLAB script. It was theorized that this was caused by constructive and destructive interference between the outputs of PA 1 and PA 2. Considering that the b_2 reflects at the PA 2 output, the b_2 reflection then adds to the a_2 wave when traveling back to the PA 1 output. This addition of the waves, going in the a_2 direction, would then interfere constructively or destructively depending on the phase difference between them. This phase difference was determined by the phase difference between a_2 and b_2, but also the travel length between the outputs of PA 1 and PA 2. Depending on the type of interference, the total reflected wave seen by the DUT could either be larger or smaller. Causing the measured load reflection coefficient Γ_{L} to be larger or smaller in amplitude based on the phase of Γ_{L}. This could cause the measured region to shift in the direction of a certain phase in the Smith chart.

By controlling the phase at which constructive/destructive interference occurs, the measured region of the Smith chart could be rotated into a region of interest. This was done by adding a through connection at the output of PA 2 in order to change the travel length between the PAs, and thereby change the phase that shifts the measured region. Different lengths of this through were tested to find a desirable region which could be used for outphasing.

3.2 Analytical Combiner S-parameter Calculations

The approach for designing the power combining antenna was to first perform analytical calculations based on the load-pull data to determine the combiner S-parameters that yield the desired load modulation behavior for maximized efficiency. Thereafter the antenna combiner was designed in CST with the aim to match these S-parameters. The design was based on the load-pull results for a fixed high input power, at which the system is intended to operate. The objective was to meet the design goals outlined in Section 2.4.2; however, other designs were also evaluated to validate the chosen approach.

To calculate the S-parameters of the combiner based on a given placement of the load modulation circles, the following approach was used: Let S_1 and S_2 represent the complex impedance points on the Smith chart where the load modulation circles intersect. For both points, the outphasing angle θ must be identical to ensure consistent phase alignment. Specifically, S_1 corresponds to the point of maximum PAE, achieved at a low outphasing angle θ_0, while S_2 corresponds to lower output power at a higher outphasing angle θ_1. Using (2.18), these conditions are translated into the following system of equations

$$\begin{cases} S_{11} + S_{12}e^{-2j\theta_0} = S_1 \\ S_{22} + S_{21}e^{j2\theta_0} = S_1 \\ S_{11} + S_{12}e^{-j2\theta_1} = S_2 \\ S_{22} + S_{21}e^{j2\theta_1} = S_2. \end{cases} \tag{3.8}$$

Then, let $\theta_1 = \theta_0 + \Delta\theta$, where $\Delta\theta$ is a parameter that needs to be optimized. Additionally, using the fact that the combiner is reciprocal, meaning $S_{12} = S_{21}$, and substituting into (3.8) results in

$$\begin{cases} S_{11} + S_{12}e^{-j2\theta_0} = S_1 \\ S_{22} + S_{12}e^{j2\theta_0} = S_1 \\ S_{11} + S_{12}e^{-j2(\theta_0+\Delta\theta)} = S_2 \\ S_{22} + S_{12}e^{j2(\theta_0+\Delta\theta)} = S_2. \end{cases} \tag{3.9}$$

Subtracting the first equation in (3.9) with the third and the second equation with the fourth yields

$$\begin{cases} S_{12}\left(e^{j2\theta_0} - e^{j2(\theta_0+\Delta\theta)}\right) = S_1 - S_2 \\ S_{12}\left(e^{-j2\theta_0} - e^{-j2(\theta_0+\Delta\theta)}\right) = S_1 - S_2. \end{cases} \tag{3.10}$$

Dividing these two equations gives

$$\frac{S_{12}\left(e^{j2\theta_0} - e^{j2(\theta_0+\Delta\theta)}\right)}{S_{12}\left(e^{-j2\theta_0} - e^{-j2(\theta_0+\Delta\theta)}\right)} = \frac{e^{j2\theta_0} - e^{j2(\theta_0+\Delta\theta)}}{e^{-j2\theta_0} - e^{-j2(\theta_0+\Delta\theta)}} = 1,$$

which implies

$$e^{j2\theta_0} - e^{-j2\theta_0} = e^{j2(\theta_0+\Delta\theta)} - e^{-j2(\theta_0+\Delta\theta)}. \tag{3.11}$$

Recall the trigonometric identity

$$\sin(\theta) = \frac{e^{j\theta} - e^{-j\theta}}{j2},$$

thus, (3.11) can be written in terms of sine-functions

$$\sin(2\theta_0) = \sin(2(\theta_0 + \Delta\theta)). \tag{3.12}$$

Solving for θ_0 given that $0 < 2\theta_0 < 2\pi$ results in 2 cases, firstly

$$2\theta_0 = 2(\theta_0 + \Delta\theta), \tag{3.13}$$

which has no non-trivial solutions, and secondly

$$2\theta_0 = \pi - 2(\theta_0 + \Delta\theta) \implies \theta_0 = \frac{\pi - 2\Delta\theta}{4}. \tag{3.14}$$

Substituting the resulting θ_0 into (3.10) and solving for S_{12} gives

$$S_{12} = \frac{S_1 - S_2}{e^{-j2\theta_0} - e^{-j2(\theta_0+\Delta\theta)}}. \tag{3.15}$$

Then, substitution (3.15) into the original expressions in (3.8) and solving for S_{11} and S_{22} yields the resulting S-parameters

$$\begin{cases} S_{11} = S_1 - S_{12}e^{j2\theta_0} \\ S_{22} = S_1 - S_{12}e^{-2j\theta_0} \\ S_{12} = \dfrac{S_1 - S_2}{e^{-j2\theta_0} - e^{-j2(\theta_0+\Delta\theta)}} \\ S_{21} = S_{12}. \end{cases} \tag{3.16}$$

By carefully choosing the phase difference $\Delta\theta$ and the optimal points $\{S_1, S_2\}$ for the PAs resulting in the highest efficiency; the S-parameters for the power combiner's two input ports are found using (3.14) and substituting into (3.16).

These equations give the desired load modulation circles, however, the output signal is also dependent on how the input waves combine in the third port. The output is given by (2.19). From this, it can be seen that the phase of S_{32} and S_{31} determines when maximum outphasing action occurs. This is when the two terms add up in phase

$$\underline{/a_1 \cdot S_{31}} = \underline{/a_2 \cdot S_{32}} \implies \theta + \underline{/S_{31}} = -\theta + \underline{/S_{32}}. \tag{3.17}$$

Ideally, this should occur at the maximum PAE point where the two circles intersect, i.e where $\theta = \theta_0$;

$$\theta_0 + \underline{/S_{31}} = -\theta_0 + \underline{/S_{32}} \implies \underline{/S_{32}} - \underline{/S_{31}} = 2\theta_0. \tag{3.18}$$

This gives maximum efficiency at the maximum output power as seen in Fig. 2.10, maximizing the system efficiency.

To evaluate the outphasing performance using the calculated S-parameters, simulations based on the load-pull data were conducted in MATLAB. By varying the phase difference $\Delta\theta$ and testing different intersection points S_1, S_2, the relative performance of each configuration was analyzed. This enabled the identification of the optimal load modulation circle placement. Details of the simulation process are provided in Section 3.4.

After determining the optimal S-parameters for the combiner, the objective was to design an antenna that matches the S-parameters defined in (3.16) and ideally also produces an output that satisfies the phase condition given in (3.18). Achieving an exact match for all these criteria may not be entirely feasible, so the design process involves finding the best possible compromise with the proposed antenna structure. As such, certain trade-offs may be necessary to balance performance and practical implementation.

3.3 Antenna Design

Before trying specific designs, a patch antenna with a center frequency of 5.4 GHz was designed. Firstly, the thickness t of the metal sheet, the height h of the substrate, and the dielectric material ε_r were chosen based on the PCBs that were available for manufacturing on *Eurocircuits*. Thereafter, the wavelength in free space was calculated using $\lambda_0 = c_0/f$ and then the dimensions L and W of the patch were retrieved using (2.21) and (2.22). Fig. 3.3 shows the dimensions of the patch antenna. The parameters denoted with subindex i refer to antenna element i (1 or 2). This notation also applies to Fig 3.4 and Fig 3.5.

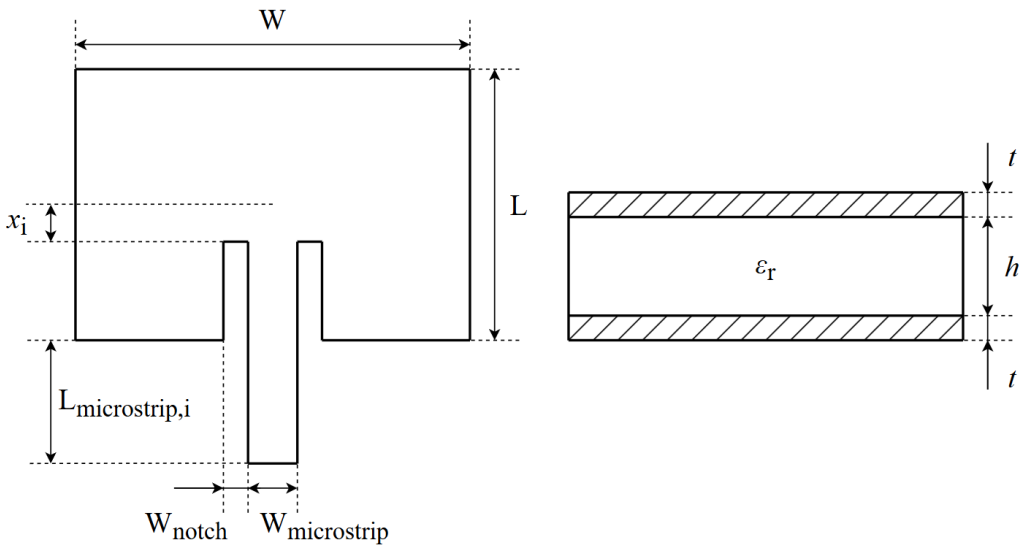

Figure 3.3: The antenna design schematic showing the dimension parameters for patch element i.

Using the parameters L, W, h, t and ε_r, the patch antenna was modeled and simulated in CST. Before defining any ports, the Eigenvalue Solver was used to verify that a resonance peak was present at 5.4 GHz; the length L of the patch had to be slightly altered to place the resonance peak at the center frequency. Thereafter, the Time Domain Solver was used to simulate the antenna by first placing a single discrete port on the symmetrical axis from the ground plane to the patch with a distance x_i from the center. Furthermore, the parameter x_i was swept from the edge to the center of the patch. The point corresponding to the lowest S_{11} value was taken as the inset point.

The width of the microstrip lines $W_{microstrip}$ was calculated using (2.23)–(2.25) and the characteristic impedance Z_0 was verified analytically using (2.26) and (2.27). The microstrip line was also verified by simulating in CST for an arbitrary length $L_{microstrip,i}$. The waveguide ports were constructed using the *Calculate port extension coefficient* macro and then the characteristic impedance of the port could be verified from the port information. After verifying the feed lines, the microstrip line was connected to the patch. The inset was designed by removing a thin strip of the metal patch next to the feed point where the microstrip line was connected.

Thereafter, the optimizer was run for the inset point x_i to minimize the reflection coefficient S_{11} at 5.4 GHz to match the port to 50 Ω.

The final design consisted of an antenna array with two elements. The two elements were placed on the same PCB with a center-to-center distance dx between the elements. As mentioned in Section 2.5.2 this will affect the input impedance. Since the design of a single element is, in isolation, matched and resonant at 5.4 GHz, the optimizer can quickly be used on multiple parameters simultaneously. Thereafter, the optimizer was run for the parameters $\{L, W, x_1, x_2, dx\}$ with the goal to minimize S_{11} and S_{22} and to match the magnitude of the S_{12}-parameter to the $|S_{12}|$ from the load-pull measurements.

3.3.1 Matching Network

A matching network was designed to match the S-parameters of the antenna to the S-parameters retrieved from the load-pull measurements. This was using an L-network containing an inductance L in series and a parallel conductance C with the antenna port. The values of these were found using the optimizer in CST for schematic simulations. The reference plane was set to the edge of the patch and transmission lines were added to the antenna ports to match the phase of the S_{12} parameters. Thereafter, the L-network, shown in Fig 3.4, was placed at the antenna ports.

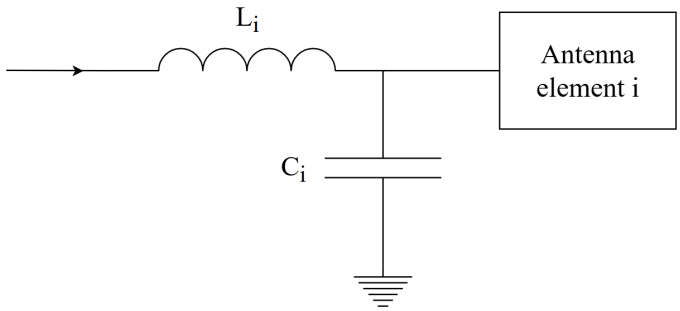

Figure 3.4: Schematic of the lumped components matching network for antenna element i.

To achieve the inductances and capacitances required for the matching, microstrip lines were used. The dimensions of these were found by setting a fixed width, W_C and W_L, of the microstrip lines for the capacitances and the inductances. Then by letting the optimizer find the length corresponding to the wanted impedances, l_Ci and l_Li were found. The microstrip line for the capacitances was connected as open-circuit stubs, and the microstrip lines for the inductances were added in series; a simple T-junction was used to connect the three transmission lines. A layout of the microstrip line matching network for one antenna element is illustrated in Fig. 3.5.

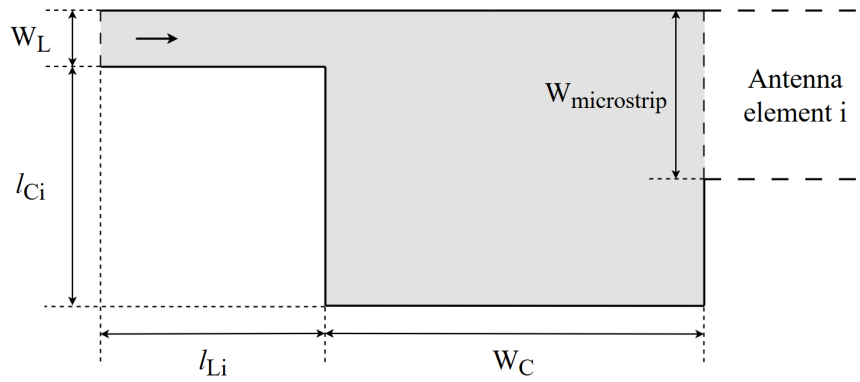

Figure 3.5: Schematic of the microstrip line matching network for antenna element i.

3.3.2 Exploratory Designs

Different patch antenna designs were modeled and simulated in CST. Firstly, the antenna proposed in [1] was modeled in CST in order to try to recreate the simulation results. Since this antenna only used one antenna with two feed lines and also used aperture-coupled feeds, the design could be flexible. If the simulation results could be recreated, then the antenna would be used for the wanted performance derived from the load-pull measurements.

Another design that was attempted was a single patch antenna with orthogonally polarized inset feed lines. This consisted of designing a patch as described above. The inset points were found by optimizing both the offset from the symmetrical axis $\{y_0, x_1\}$ and the offset from the center toward the edge $\{x_0, y_1\}$. The optimization goals were $\min |S_{11}|$ and $\min |S_{22}|$ at the frequency 5.4 GHz. Thereafter, the microstrip lines were connected with an inset at these points. Finally, an attempt to match this to 50 Ω was made using the optimizer. Further discussion regarding the exploratory designs can be found in Appendix A.1.

3.4 Outphasing Simulations

To evaluate the performance of the outphasing system, simulations based on the load-pull results and antenna designs were performed in MATLAB and CST. The simulations were carried out in two stages. Firstly, as mentioned at the end of Section 3.2 they were used to help determine the optimal selection of the analytically calculated S-parameters. Secondly, the simulations were repeated using the realized antenna design models in CST, evaluating the practical performance of the system.

Since the load-pull results consisted of discrete data points, interpolation was required to enable continuous analysis over the Smith chart. The interpolation was performed using the MATLAB `griddata` function, giving a piecewise linear approximation of the measured parameter values across the entire measured region on the Smith chart.

Using the 2-port S-parameters of the combiner inputs, the load modulation circles, Γ_{PA_1} and Γ_{PA_2} were predicted using (2.18) as described in Section 2.4.1. By sweeping the outphasing angle, parameter values were extracted from the interpolated data along the circles. This data was then used to analyze the system's output power $P_{\mathrm{out,tot}}$, and total PAE as a function of the outphasing angle. The PAE was also evaluated as a function of power back-off levels to assess the outphasing system's efficiency in scenarios involving amplitude modulation, such as in QAM systems.

To evaluate the output of the system, the magnitude of the input waves to the combiner at each outphasing angle was obtained from the interpolated load-pull data. It is important to note that this magnitude is not equivalent to $\sqrt{2 \cdot P_{\mathrm{out,PA}}}$, as that expression includes both the forward and reflected components from the load, see (2.5). Instead, the magnitude of the measured output wave from the PAs (denoted as the b_2 wave in Fig. 3.2) was used for each predicted load impedance. Applying the differential outphasing angle θ as in (2.14), the inputs to the combiner were given by

$$a_{1,\mathrm{comb}} = |b_{2,\mathrm{PA}_1}(\theta)| \cdot e^{j\theta}, \qquad a_{2,\mathrm{comb}} = |b_{2,\mathrm{PA}_2}(\theta)| \cdot e^{-j\theta}. \tag{3.19}$$

Power back-off is given in dB and defined as

$$P_{\mathrm{Back\text{-}off,dB}}(\theta) = 10 \cdot \log_{10}\left(\frac{P_{\mathrm{out,tot}}(\theta)}{\max\left(P_{\mathrm{out,tot}}(\theta)\right)}\right). \tag{3.20}$$

The total power-added efficiency for the outphasing system is computed as

$$\mathrm{PAE}_{\mathrm{tot}}(\theta) = \frac{P_{\mathrm{out,tot}}(\theta) - 2P_{\mathrm{in,PA}}}{P_{\mathrm{DC}_1}(\theta) + P_{\mathrm{DC}_2}(\theta)}. \tag{3.21}$$

Here, both the input RF power and DC power consumption of the two amplifier branches are included.

Determining the output power level and thus total PAE of the system when using an antenna as a combiner is however not straightforward. Since power combining occurs in free space, the received power decreases with distance from the transmitters, following Friis' equation (2.29). As a result, the measured output power depends on the position of the receiving antenna. To account for this, the system was evaluated using normalized output power and PAE levels, which provide a relative measure of how the output power and efficiency vary with the outphasing angle, independent of distance.

3.4.1 Analytical S-parameter Simulations

To evaluate the system performance using the calculated S-parameters from Section 3.2 the relative output power was evaluated using approximations of the S_{31} and S_{32} parameters. Different configurations of $\Delta\theta$, S_1 and S_2 were tested, along with different phase differences between S_{32} and S_{31}. These configurations were compared against each other and a fully isolated reference case matched to the maximum

PAE point from the load-pull. In the fully isolated case, there exists no coupling between the two ports (S_{21} and $S_{12} = 0$) and thus no load modulation action occurs.

As only relative power levels were considered, the magnitudes of S_{31} and S_{32} were set to arbitrary but equal values across all configurations, ensuring a fair comparison of the relative performance. The output b_3 wave was then calculated using (2.19). The combined output power $P_{\text{out,tot}}$ was calculated using the same approach as in (2.5), but since there is no incident wave at the output port ($a_3 = 0$), it simplifies to

$$P_{\text{out,tot}} = \frac{|b_3|^2}{2}. \tag{3.22}$$

This was then normalized to the highest output power across all evaluated cases. Finally, the relative efficiency at different power back-off levels was assessed using (3.20) and (3.21). The configuration that yielded the highest overall and back-off efficiency was selected as the target S-parameters for the power combining antenna.

3.4.2 Antenna Combiner Simulations

The outphasing simulations for the realized antenna designs were conducted in CST using the Schematic simulator. Using the a-coefficients as stated in (3.19) as the excitation coefficients for the two ports, the different outphasing angles could be simulated. The coefficients corresponding to an outphasing angle of 0 to 180° with a step size of 15° were used for both the lumped component matching network as well as the microstrip line matching network. The accepted input power was then calculated by

$$P_{\text{in,ant}} = \frac{1}{2}\left[\boldsymbol{a}^H\boldsymbol{a} - (\mathbf{S}\boldsymbol{a})^H(\mathbf{S}\boldsymbol{a})\right] \tag{3.23}$$

where $\boldsymbol{a}$ is the 2×1 vector of the excitation coefficients and $\mathbf{S}$ is the 2×2 matrix for the simulated scattering parameters of the antenna with the matching network.

The IEEE gain was retrieved from the CST simulation of the system for the different excitations by taking the broadside point in the linear scale for the φ-component. Using (2.30) the non-normalized proportionality of the received power in broadside was calculated.

The received power values were then normalized by the maximum output power across both combiner designs. Thereafter, the relative efficiency at different power back-off levels was evaluated using (3.20) and (3.21), enabling a direct comparison of the designs' performance, both in regards to total output power and efficiency at different back-off levels.

4

Results

This chapter presents both the intermediate results used in the design of the outphasing system and the simulation results evaluating its performance. The results from load-pull measurements, combiner S-parameter calculations, antenna design, and outphasing simulations are included here.

4.1 Load-Pull

The characteristics of the PA parameters PAE and P_{out} are presented in Fig. 4.1. The plots indicate which load impedance yields the maximum value for each parameter and how they vary in the measured region of the Smith chart.

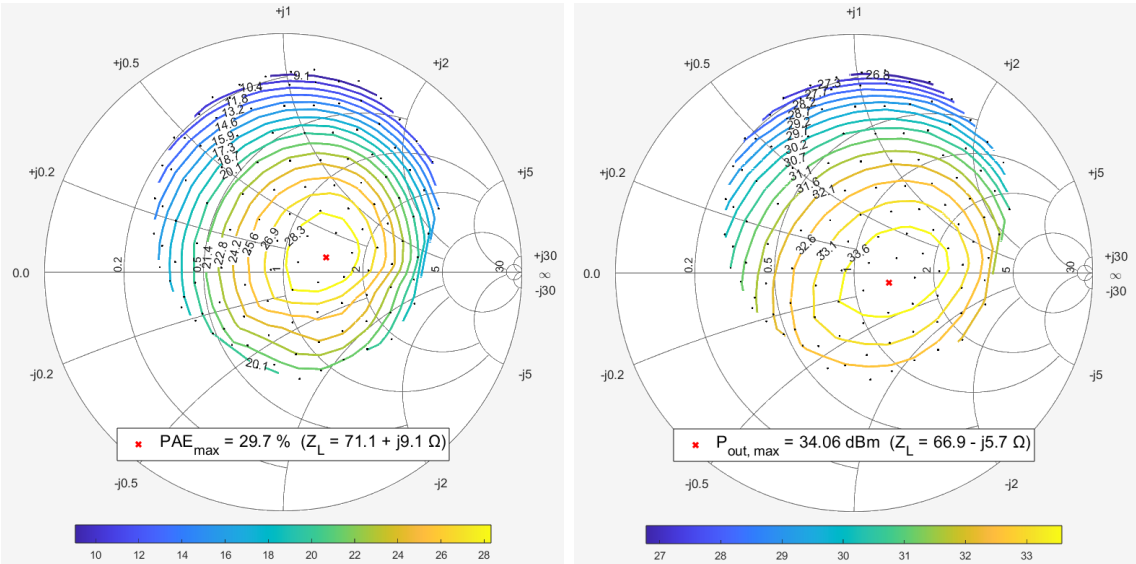

(a) PAE [%] contour plot with maximum marked.

(b) P_{out} [dBm] contour plot with maximum marked.

Figure 4.1: Load-pull results illustrating how the parameters PAE and P_{out} change depending on the load impedance presented to the PA, with an average input power of 3.93 dBm.

These plots were used to determine the optimal placement of the load modulation circles for the PAs in outphasing.

4.2 Optimal Combiner S-parameters

This section presents the selection of the combiner S-parameters to which the antenna is matched. Based on the initial antenna design, it was observed that a maximum coupling of approximately −11 dB could be achieved. Consequently, the magnitudes of S_{12} and S_{21} were constrained to this value when determining the optimal parameters. To determine the optimal parameters, the following cases were evaluated through the MATLAB simulations:

1. Circle placement along the symmetry line, as described in Section 2.4.2, with the phases of S_{31} and S_{32} set to 0°.
2. Circle placement along the symmetry line, with the phases of S_{31} and S_{32} chosen according to (3.18).
3. Circle placement not centered on the symmetry line, with the phases of S_{31} and S_{32} set to 0°.
4. A fully isolated reference case, matched to the maximum PAE point of the amplifiers. In this case, $S_{21} = S_{12} = 0$, resulting in no load modulation circles.

Fig. 4.2 shows the different placement of the circles along with the load-pull data and an approximate line of output power symmetry.

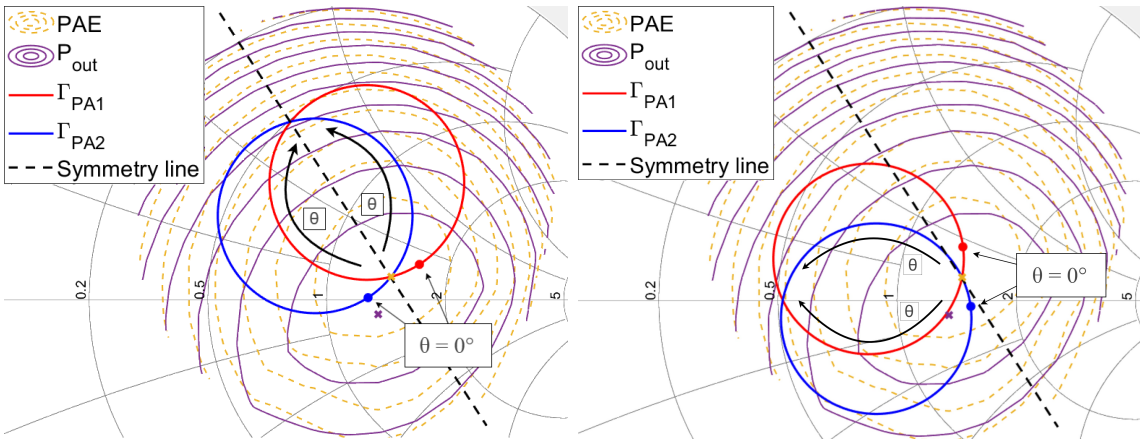

(a) Circle placement over the line of output power symmetry, case 1 and 2.

(b) Off-symmetry placement of load modulation circles, case 3.

Figure 4.2: Analytical outphasing load modulation circles overlaid on PAE and P_{out} contours. The figure illustrates the placement of the circles relative to the PA characteristics. The dots mark the point corresponding to $\theta = 0°$, and as θ increases, the load impedances trace the circles in the direction of the arrows.

The normalized power added efficiency for the four cases is plotted against the power back-off level in Fig. 4.3 below.

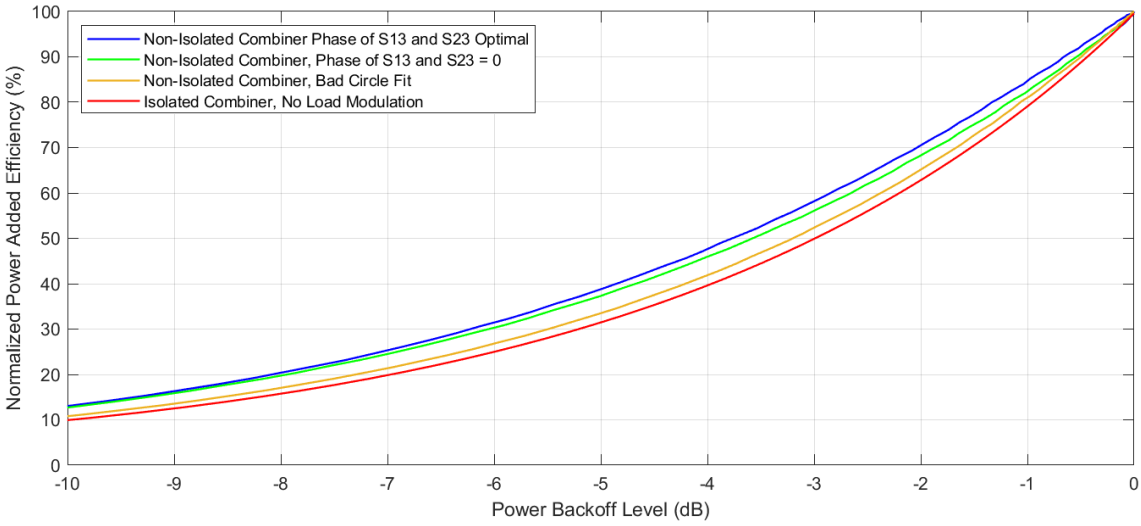

Figure 4.3: Normalized Power added efficiency vs. back-off power level for the 4 different picks of S-parameters where $0° < \theta < 90°$.

From this, it can be concluded that the circle fit in Fig. 4.2a with phase of S_{31} and S_{32} according to (3.18) results in the best efficiency at back-off. Therefore, this configuration was chosen for the final design. The resulting S-parameters for this circle placement are displayed in Table 4.1.

Table 4.1: S-parameters for the selected combiner design in rectangular and polar form.

Parameter	Rectangular Form	Polar Form
S_{11}	$0.1131 + j0.3288$	$0.35\underline{/71.02°}$
S_{12}	$0.1485 - j0.2298$	$0.27\underline{/-57.12°}$
S_{21}	$0.1485 - j0.2298$	$0.27\underline{/-57.12°}$
S_{22}	$-0.0319 + j0.2350$	$0.24\underline{/97.74°}$

The corresponding θ_0, from these S-parameters, where in-phase outphasing should occur is $\theta_0 = 9.2°$. As a result, these S-parameters, along with the corresponding phase conditions for S_{31} and S_{32} as defined in (3.18)

$$\underline{/S_{32}} - \underline{/S_{31}} = 2\theta_0 = 18.4° \tag{4.1}$$

were used as the target when designing the antenna.

4.3 Antenna Design

The antenna elements, shown in Fig. 3.3, have the dimensions as presented in Table 4.2, where the dimensions $W_{\text{microstrip}}$, $L_{\text{microstrip,1}}$ and $L_{\text{microstrip,2}}$ of the microstrip feed were found after optimizing the lumped component matching network. The elements were placed with a distance of $dx = 21.36$ mm between the center of the two

ports. Furthermore, the patch antenna array was placed over a ground plate with the dimensions 62.954×41.592 mm^2.

Table 4.2: Dimensions for the patch antenna elements without matching network.

Parameter	**Value [mm]**
L	13.842
W	16.218
W_{notch}	0.570
$W_{\text{microstrip}}$	1.139
$L_{\text{microstrip,1}}$	1.670
$L_{\text{microstrip,2}}$	4.364
x_1	1.597
x_2	0.000
t	0.018
h	0.508

The S-parameters for the antenna array before connecting the matching network and the co-polar embedded element pattern for port 1 are shown in Fig. 4.4. The radiation pattern for the second element is anti-symmetrical to the first element pattern.

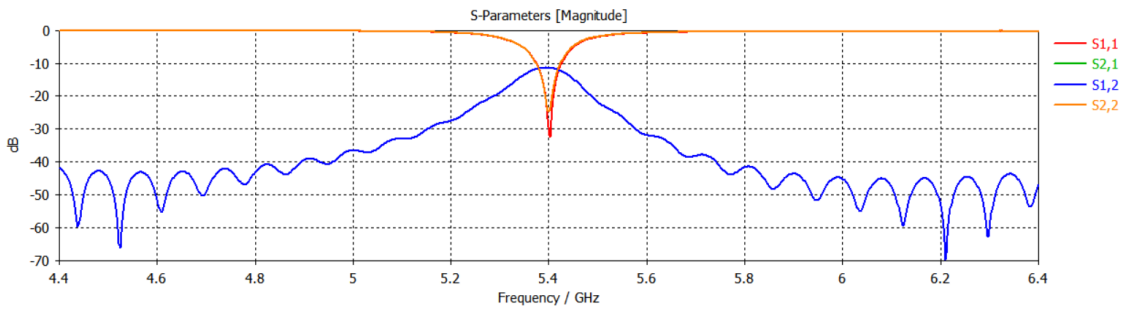

(a) S-parameters over frequency for the two-element antenna array without matching network.

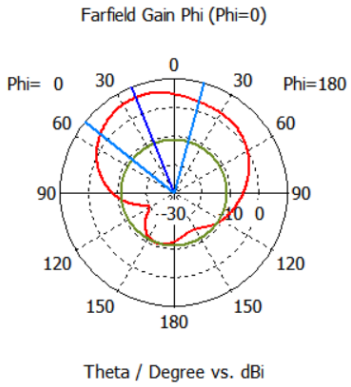

(b) Co-polar radiation pattern of the antenna without matching network.

Figure 4.4: S-parameters and co-polar embedded element pattern for the antenna array without matching networks for the ports.

As seen, the antenna ports are well matched to 50 Ω, reflection coefficients below -20 dB, and the coupling coefficients are approximately -11.4287 dB at 5.4 GHz.

4.3.1 Lumped Component Matching Network

As described in Section 3.3.1 the matching network was first designed using lumped components in an L-network, as shown in Fig. 3.4. Running the optimizer resulted in the inductance L_1 and capacitance C_1 for port 1, along with L_2 and C_2 for port 2. These values are presented in Table 4.3.

Table 4.3: Values for the lumped component matching networks at ports 1 and 2.

Parameter	Value
L_1	1.462 [nH]
C_1	0.173 [pF]
L_2	1.328 [nH]
C_2	0.310 [pF]

The resulting S-parameters are shown in Table 4.4.

Table 4.4: S-parameters of the antenna with lumped component matching network in rectangular and polar form.

Parameter	Rectangular Form	Polar Form
S_{11}	$0.1131 + j0.3287$	$0.35\underline{/71.01°}$
S_{12}	$0.1369 - j0.2051$	$0.25\underline{/-56.28°}$
S_{21}	$0.1369 - j0.2051$	$0.25\underline{/-56.28°}$
S_{22}	$-0.0319 + j0.2350$	$0.24\underline{/97.73°}$

Comparing these results with the desired parameters in Table 4.1 it can be concluded that the matching using this approach was rather successful with S_{11} and S_{22} being matched almost perfectly, and S_{12} and S_{21} deviating by about 9%.

4.3.2 Microstrip Line Matching Network

Running the optimizer, for the microstrip matching network shown in Fig. 3.5, gave the dimensions l_{L1}, l_{C1}, l_{L2} and l_{C2}. Where the transmission line width for the inductance was fixed to $W_{\mathrm{L}} = 0.1$ mm and the width for the capacitance was fixed to $W_{\mathrm{C}} = 3$ mm. The dimension values are presented in Table 4.5.

Table 4.5: Dimensions of the microstrip line matching networks at ports 1 and 2.

Parameter	Value [mm]
W_{L}	0.1
W_{C}	3
l_{L1}	0.819
l_{C1}	0.509
l_{L2}	0.873
l_{C2}	1.145

The resulting S-parameters are presented in Table 4.6.

Table 4.6: S-parameters of the antenna with microstrip matching network in rectangular and polar form.

Parameter	Rectangular Form	Polar Form
S_{11}	$0.0226 + j0.0120$	$0.03\underline{/27.97°}$
S_{12}	$-0.0395 + j0.2653$	$0.27\underline{/98.47°}$
S_{21}	$-0.0395 + j0.2653$	$0.27\underline{/98.47°}$
S_{22}	$0.0235 + j0.0530$	$0.06\underline{/66.09°}$

In this case, the matching was less successful. Compared to the desired values in Table 4.1, the acquired S-parameters from the microstrip matching deviate a lot.

This is mainly due to the transmission lines not being able to achieve the impedance without unrealistic widths in the current type of matching network.

4.4 Outphasing Simulations

In this section, the results from the outphasing simulations based on the CST antenna designs are presented. Firstly, the resulting load modulation on the PAs is evaluated based on the S-parameters of the two designed antenna combiners. Thereafter, radiation patterns and the antenna gain at broadside for different outphasing angles are presented. Finally, the overall power output and efficiency of the system are evaluated.

4.4.1 Resulting Load Modulation on the PAs

The corresponding load modulation circles for the antenna with the lumped component matching network and the microstrip line matching network are shown in Fig. 4.5. Quite a large discrepancy can be seen between the two cases due to the microstrip line matching network not being able to achieve the wanted S-parameters with the current design of the matching network.

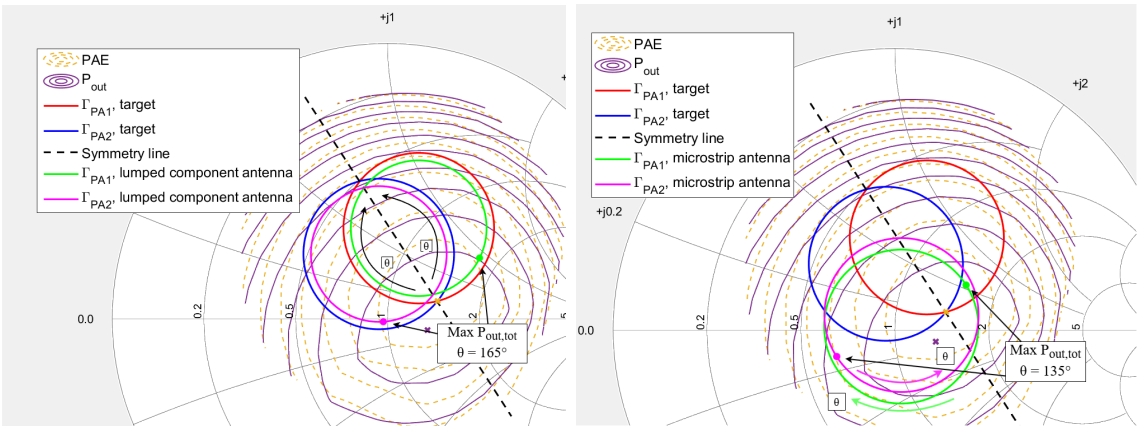

(a) Resulting load modulation circles of the lumped component matching antenna **(b)** Resulting load modulation circles of the microstrip matching antenna

Figure 4.5: Predicted load modulation circles for the different antenna feeding configurations compared against the target design. The dots indicate the point of maximum system output power. As θ increases, the load on the PAs traject along the circles in the direction of the arrows.

The maximum system output power is achieved at $\theta = 165° \pm 180 \cdot n$ for the lumped component antenna and at $\theta = 135° \pm 180 \cdot n$ ($n \in \mathbb{N}$) for the microstrip antenna (note that the output power is periodic with a period of 180°).

The resulting output waves from the PAs along the predicted load modulation circles in Fig. 4.5 are plotted as a function of the outphasing angle in Fig. 4.6 below. From this data, values were sampled at 15° intervals and used as the excitation signals for

the antenna in CST, following the formulation in (3.19). The specific values used for exciting the antenna ports are provided in Appendix A.2.

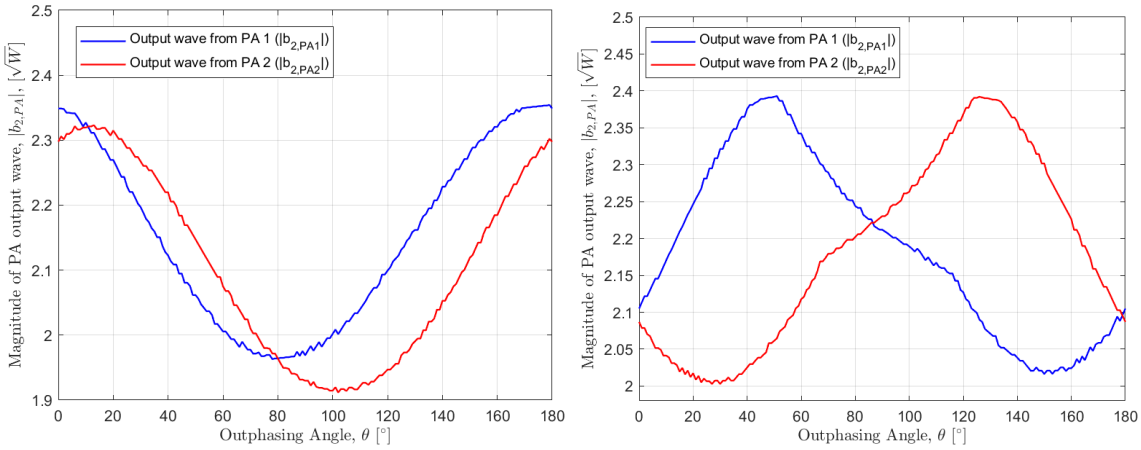

(a) Magnitude of the output waves the PAs using the lumped component antenna

(b) Magnitude of the output waves the PAs using the microstrip antenna

Figure 4.6: Output waves of the PAs at different outphasing angles which corresponds to the magnitude of the input waves of the antenna combiner, $|a_{1,\text{comb}}|$ and $|a_{2,\text{comb}}|$.

It can be seen that the lumped component antenna satisfies the condition of equal output powers quite well, whereas in the microstrip case, the magnitude of the output waves from the PAs deviates quite a bit from each other.

4.4.2 Radiation Patterns at Outphasing

For the antenna array with lumped components matching network, the lowest gain at broadside was achieved for the outphasing angle $\theta = 75°$ and the highest gain was received at $\theta = 165°$, the maximum gain is also expected at $\theta = -15°$ due to the periodicity of outphasing. The radiation patterns at different outphasing angles for the lumped component antenna are presented in Fig. 4.7.

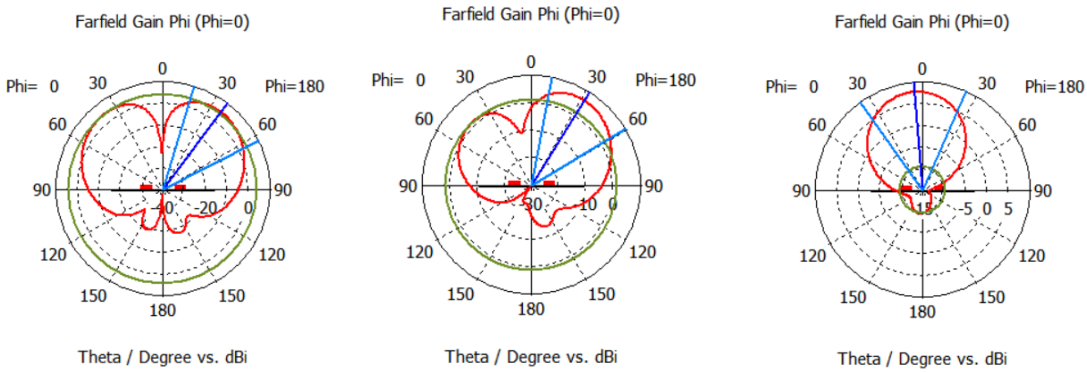

(a) Total radiation pattern for the outphasing angle $\theta = 75°$.

(b) Total radiation pattern for the outphasing angle $\theta = 90°$.

(c) Total radiation pattern for the outphasing angle $\theta = 165°$.

Figure 4.7: Total radiation patterns (φ constant) for the antenna with the lumped component matching network for the lowest, intermediate, and maximum gain in broadside.

The total radiation patterns, shown in Fig. 4.8, for the microstrip line matching antenna the lowest and highest gain were at $\theta = 60°$ and $\theta = 150°$ respectively. The maximum gain is also expected at $\theta = -30°$ due to symmetry.

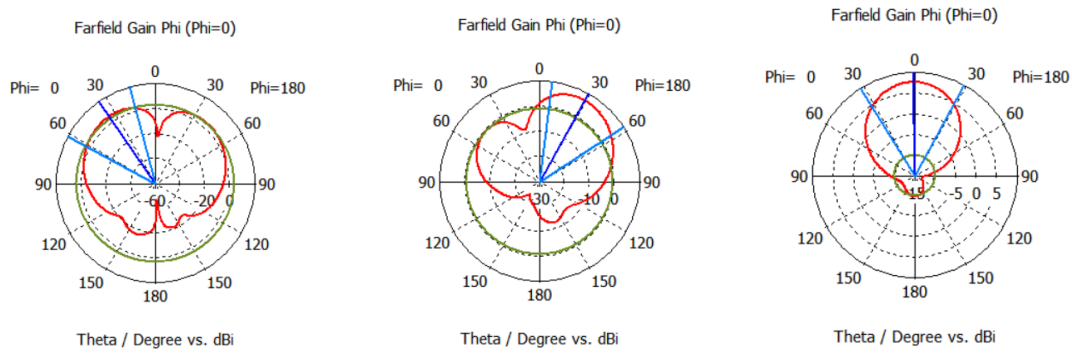

(a) Total radiation pattern for the outphasing angle $\theta = 60°$.

(b) Total radiation pattern for the outphasing angle $\theta = 90°$.

(c) Total radiation pattern for the outphasing angle $\theta = 150°$.

Figure 4.8: Total radiation patterns (φ constant) for the antenna with the microstrip line matching network for the lowest, intermediate, and maximum gain in broadside.

The difference in the outphasing angles compared to the lumped component case is due to the deviating S-parameters. Consequently, the excitations are different which results in the angles for maximum and minimum gain being shifted by a few degrees. The antenna IEEE gain at broadside for the antennas with the two different matching networks is presented in Fig. 4.9.

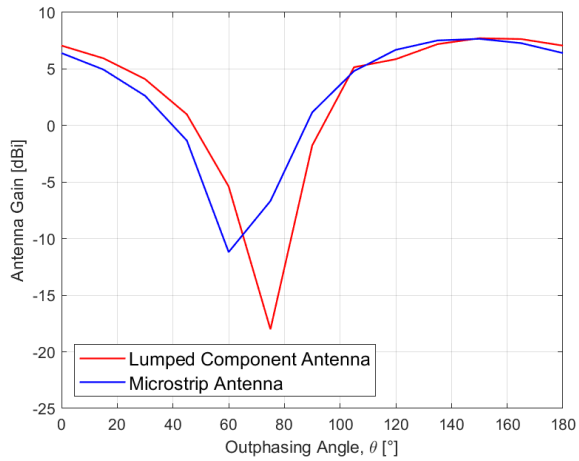

Figure 4.9: IEEE Gain of the antennas at broadside as a function of the outphasing angle θ.

Due to the low resolution of 15°, the full notch for the microstrip line matched antenna is not shown in the figure. The gain is expected to reach the same maximum gain value before $\theta = 0$ as well but is not shown in the figure due to only $0 \leq \theta \leq 180°$ being investigated.

4.4.3 Total Power and PAE

The normalized received power, shown in Fig. 4.10, varies periodically in an approximate sinusoidal shape. This is due to the beam being steered away from broadside and low power being transmitted in broadside. For larger scan angles, this results in a side lobe which increases in intensity until finally becoming the main beam and then being steered back to broadside.

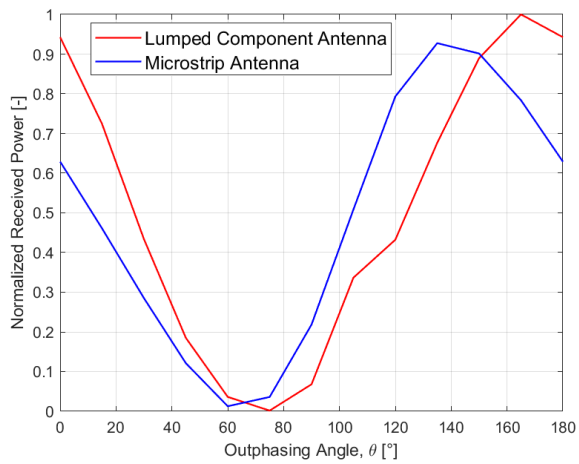

Figure 4.10: Normalized received power at broadside against the outphasing angle θ.

The lumped component matching network resulted in a higher received power than the microstrip line case. As shown in the tables in Appendix A.2 the peak power

from the PAs to the inputs of the antennas is lower for the microstrip line case compared to the lumped component case for the angles where the beam is steered to broadside, which is the reason for the lower received power level.

Fig. 4.11 shows the total PAE of the system compared to the power back-off level. As seen in Fig. 4.10, the same power level is achieved twice as θ sweeps from 0° to 180°, resulting in a curve that loops back on itself.

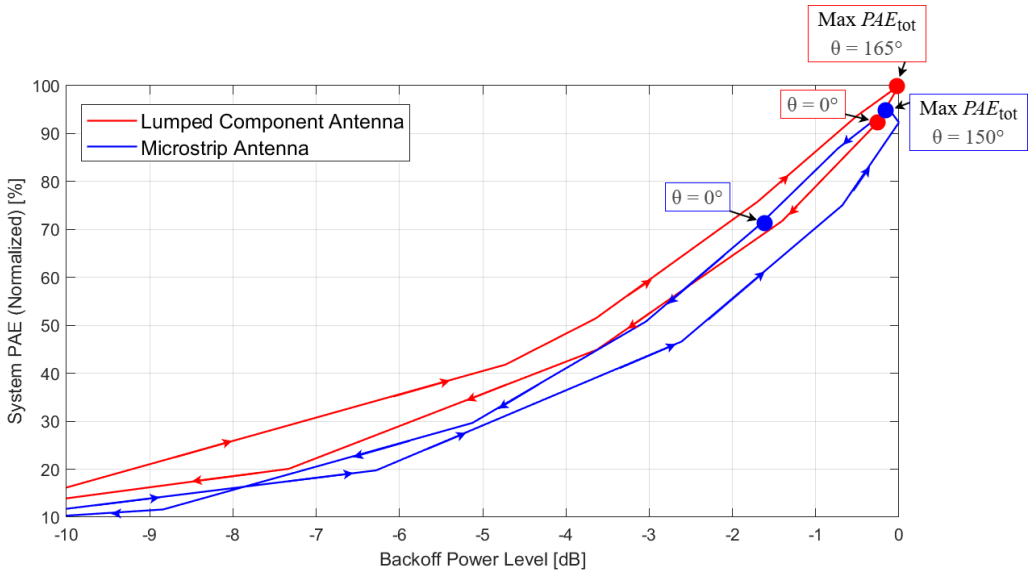

Figure 4.11: Normalized total PAE versus back-off power level in dB for $0° < \theta < 180°$. As θ increases, the plots trace the curve in the direction indicated by the arrows.

Overall, the efficiency is higher for the better-matched lumped component case compared to the microstrip case. Furthermore, it can be observed that the maximum efficiency points appear at the same outphasing angle as the maximum antenna gain. This occurs because, at these angles, the two signals combine in-phase at broadside, and maximum outphasing action is achieved. Consequently, less power is lost in the combining step, resulting in improved overall system efficiency at this angle. As previously discussed, the goal was to achieve this at the maximum PAE point, where $\theta = \theta_0 = 9.2°$. However, none of the current antenna designs fully met this criterion, with the lumped component case coming closest, deviating by 24.2°.

5
Discussion

The results from the project, and some of the methods used, are discussed in this chapter. Discussions on the PAs, load-pull setup, antenna design, and outphasing simulations are held here. Suggestions for future work in these areas are presented as well.

5.1 Power Amplifiers

The QPA9501 PAs were used to show the potential benefits of using the outphasing technique presented in this project. However, they were not ideal for this purpose. As mentioned previously, the outphasing technique can take advantage of highly efficient nonlinear amplifiers. However the PAs in this project behave pretty linearly, and only some nonlinear effects were caused by driving them with a large input power. This is because the PAs operate mostly in the linear region as seen in the datasheet, where the 1 dB compression point occurs near the maximum output power of the amplifiers [24]. This could also explain the low efficiency seen in the PAE results in Fig. 4.1a, where the maximum PAE is 29.7 %. To accurately evaluate the performance potential of outphasing with nonlinear amplifiers, PAs with stronger nonlinearities and higher efficiencies may be more suitable.

The amplifiers are designed for 50 Ω, which also can be seen in the plots of Fig. 4.1. This means that they are mismatched during load modulation, which results in a decrease in the efficiency of the system. Ideally, to achieve the maximum efficiency from the amplifiers in an outphasing system, the PAs should be co-designed with the antenna.

5.2 Load-Pull Setup

The load-pull setup was constructed only to fulfill the purposes of this project, as presented in Section 3.1. However, there are some potential areas of improvement if measurements need to be conducted with more control and precision when testing a load. One aspect is the influence that the DUT exerts on the setup.

During the measurements, PA 2 was not isolated from the output signal of the DUT. This caused PA 2 to be load modulated in the same way as the DUT. Thus, PA 2 was presented with a large load impedance when sending the generated reflected wave. Which in turn altered the output of the PA, similar to how the DUT changes

output as seen in Fig. 4.1b. This alteration was not accounted for when picking points on the Smith chart and is different from the shift presented in Section 3.1.4. Therefore, the measured load impedances were slightly different and not as evenly spaced as the ones picked in MATLAB. This relatively small change can be seen in the load-pull results. However, this did not affect the measured characteristics. Isolating PA 2 from the DUT output could improve the precision and control of generating loads. One way to do this could be to add a circulator at the output of PA 2, which would divert the output of the DUT from PA 2 to a termination. This could also fix the shift of the measurement region as presented in Section 3.1.4.

5.3 Antenna Design

The antenna array was only modeled to be used for simulations, this was mainly due to exploratory designs not yielding the wanted results and other time constraints. This made it possible to use more precise values for the circuit components and not having to investigate the effect of tolerances in the dimensions. Therefore, the results in connection with the antenna are aimed at proof-of-concept and risk being too ideal.

Large discrepancies can be seen between the matching network composed of lumped components and the network consisting of microstrip lines. This can possibly be remedied by utilizing a more sophisticated matching network, such as a multi-stub network or other techniques to construct the required inductances and capacitances instead of the proposed microstrip line matching network. Furthermore, the lumped component network might be hard to realize at this frequency band due to the resonance frequency of commercially used components usually being well below 5.4 GHz. The very specific values of the inductance and capacitance required for the matching can generally not be found for commercially available components.

In this project, only patch antennas have been analyzed. Other antenna types might be more suited for this type of application. In [3] a half-loop antenna was used for outphasing, but monopoles and dipoles could also be possible; aperture antennas might also be suitable but might result in a physically larger array compared to the other cases.

Since the antenna was not manufactured and measured in an anechoic chamber, the non-idealities e.g. the dielectric material and conductors could not be considered. The tolerances for the dimensions of the antenna might also change the resonance frequency. These factors might significantly alter the S-parameters for the antenna as well as add ohmic losses not considered. Furthermore, a receive antenna will be required for measurements. This antenna has its own gain that has to be taken into account and will also introduce re-radiation and further power losses. Furthermore, the matching network might also differ due to the aforementioned tolerances.

5.4 Outphasing Simulations

From the results, it can be concluded that using an antenna array as a power combiner in an outphasing modulator system is possible. However, some improvements could be made to increase its efficiency. Firstly, it can be seen from Fig. 4.11 that better matched S-parameters do result in higher efficiency. Thus, a better matching network using microstrip lines needs to be explored for better implementation at higher frequencies. Furthermore, as can be seen in Fig. 4.7 and Fig. 4.8, the outphasing angles for maximum and minimum power deviate from the desired angles $\theta = \theta_0$ and $\theta = \theta_0 + 90°$ respectively. A possible solution could be to increase the transmission line length $L_{\text{microstrip},1}$ and decrease the length $L_{\text{microstrip},2}$ to compensate for the deviation in outphasing angle without radically changing the phase of S_{21}, this should then satisfy (3.18). For the antenna with the lumped component matching network, approximately $\theta_0 + 15°$ has to be compensated. For the antenna with microstrip matching, approximately $\theta_0 + 30°$ has to be compensated. As previously stated, the resolution should be increased to resolve the ambiguity before changing the transmission line length. It is important to verify that the other S-parameters are unaffected by this change in length. Furthermore, a length corresponding to half a wavelength could be added to make room for sockets for physical ports.

For the gain over outphasing angle plot in Fig. 4.9, there is some ambiguity for the outphasing angles resulting in the notch in the gain. There could exist a lower value for the antenna with the microstrip matching network between the outphasing angle 60° and 75° that is not shown. The remedy could be to increase the resolution to 1°. This was not done due to the amount of time to either simulate it by manually entering the excitations in CST or implement a MATLAB script, using a CST interface such as *TCSTInterface*, that would perform the simulations.

For the outphasing angles where the beam is steered away from broadside, the power would be transmitted to the surrounding environment. This would significantly interfere with potential surrounding receivers or signals. This might make it difficult to implement in environments with multiple receive and transmit systems.

While simulations of the outphasing system are intended to approximate the behavior of a practical implementation, assumptions and simplifications limit their accuracy. The simulated load modulation was simplified given the assumption that the load modulation circles were placed symmetrically on the output power symmetry line in Fig. 4.2a. The output power of both PAs was then approximated to be identical at all times. This can be seen in the equations of Section 2.4.1. Where (2.18) assumes identical output amplitude A of both PAs. In practice, as shown in (2.17), the presented load impedances Γ_{PA1} and ΓPA_2 depend on the ratio of the PA output signals, A_1 and A_2. However, this ratio is itself influenced by the load impedances, resulting in a feedback loop.

To improve the simulations, an iterative calculation process could be used as presented in [25]. Using this approach, calculations of the load impedance were iterated

until the difference in calculated output power, based on the load-pull data, between iterations was smaller than -13 dB. This process is something that could have improved the accuracy of the outphasing simulations in this project. Ultimately, however, to evaluate the actual performance of the system, the physical outphasing setup should be assembled and measured.

6
Conclusion

The project designed and simulated an outphasing system with a two-element patch antenna array as the power combiner. An active vector-receiver load-pull setup was successfully constructed and calibrated using an FPGA board, bi-directional couplers, and an 8-term SOLT calibration model. This setup was used to characterize the PAs. From the load-pull results, the PAs showed a maximum efficiency of 29.7 % and a maximum output power of 34.06 dBm close to 50 Ω for an input power of 3.93 dBm. These characteristics allowed for the ideal two-port S-parameters of the power combining antenna array to be determined. It was shown that an antenna array consisting of patch antenna elements matched to these S-parameters was able to utilize the coupling between the input ports for improved efficiency. Using lumped components, the inputs of the antennas were successfully matched to the desired S-parameters with a relative error of around 9% for the coupling and almost no relative error for the reflection coefficients. When using microstrip lines, however, the matching network could not provide sufficient matching in its current configuration, resulting in worse efficiency and lower power output than for the lumped component case.

In conclusion, using an antenna array as a power combiner in an outphasing system shows promise. However, future work that could improve the performance includes designing better matching networks and utilizing more efficient nonlinear PAs. Furthermore, the system would need to be tested and evaluated through physical measurements.

Bibliography

[1] D. Tresnawan, P. Smulders, B. van Ark, and A. B. Smolders, "Linear LINC transmitters using dual-polarized power-combining antennas", in *12th European Conference on Antennas and Propagation (EuCAP 2018)*, 2018, pp. 1–4. DOI: 10.1049/cp.2018.1164.

[2] S. Gao and P. Gardner, "Integrated antenna/power combiner for LINC radio transmitters", *IEEE Transactions on Microwave Theory and Techniques*, vol. 53, no. 3, pp. 1083–1088, 2005. DOI: 10.1109/TMTT.2005.843491.

[3] F. P. van der Wilt, E. Habekotté, and A. B. Smolders, "A non-isolated power-combining antenna for outphasing radio transmitters", *IEEE Transactions on Antennas and Propagation*, vol. 64, no. 2, pp. 761–766, 2016. DOI: 10.1109/TAP.2015.2504456.

[4] S. C. Cripps, *RF Power Amplifiers for Wireless Communication*, Second edition. Artech House, 2006.

[5] M. Litchfield, T. Reveyrand, and Z. Popović, "X-band outphasing power amplifier with internal load modulation measurements", in *2014 44th European Microwave Conference*, 2014, pp. 1428–1431. DOI: 10.1109/EuMC.2014.6986714.

[6] M. Litchfield, T. Reveyrand, and Z. Popović, "Load modulation measurements of X-band outphasing power amplifiers", *IEEE Transactions on Microwave Theory and Techniques*, vol. 63, no. 12, pp. 4119–4129, 2015. DOI: 10.1109/TMTT.2015.2495127.

[7] Rohde & Schwarz. "Amplifier characterization using load pull". [Accessed: Apr. 2025]. (2020), [Online]. Available: https://www.rohde-schwarz.com/se/applications/amplifier-characterization-using-load-pull-application-card_56279-922304.html.

[8] H.-S. Lui, H. T. Hui, and M. S. Leong, "A note on the mutual-coupling problems in transmitting and receiving antenna arrays", *IEEE Antennas and Propagation Magazine*, vol. 51, no. 5, pp. 171–176, 2009. DOI: 10.1109/MAP.2009.5432083.

[9] G. Collins and D. W. Runton, "Nonlinear analysis of power amplifiers", *Microwave Journal*, Sep. 2007, [Accessed: Apr. 2025]. [Online]. Available: https://www.microwavejournal.com/articles/5308-nonlinear-analysis-of-power-amplifiers.

[10] S. Cripps, "Amplifier classes, A to S", in *Handbook of RF and Microwave Power Amplifiers* (The Cambridge RF and Microwave Engineering Series), J. L. B. Walker, Ed., The Cambridge RF and Microwave Engineering Series. Cambridge University Press, 2011, pp. 159–187.

[11] Electronics Tutorials. "Amplifier classes". Accessed: 2025-04-15. (2024), [Online]. Available: `https://www.electronics-tutorials.ws/amplifier/amplifier-classes.html`.

[12] M. Albulet, *RF Power Amplifiers*. The Institution of Engineering and Technology, 2001. DOI: `10.1049/SBEW030E`. eprint: `https://digital-library.theiet.org/doi/pdf/10.1049/SBEW030E`. [Online]. Available: `https://digital-library.theiet.org/doi/abs/10.1049/SBEW030E`.

[13] B. A. Forouzan, *Data Communications and Networking*, 4th ed. McGraw-Hill Education, 2007, pp. 141–152, ISBN: 9780073376226.

[14] B. Zhang, Y. Qu, and M. Chen, "Simulation and performance study of quadrature amplitude modulation and demodulation system", *IOP Conference Series: Materials Science and Engineering*, vol. 782, no. 4, p. 042 048, Mar. 2020. DOI: `10.1088/1757-899X/782/4/042048`.

[15] F. M. Ghannouchi and M. S. Hashmi, "Load-pull techniques and their applications in power amplifiers design (invited)", in *2011 IEEE Bipolar/BiCMOS Circuits and Technology Meeting*, 2011, pp. 133–137. DOI: `10.1109/BCTM.2011.6082765`.

[16] S. Dudkiewicz, "Vector-receiver load pull measurements", *Microwave Journal*, Feb. 2011, [Online]. Available: `https://www.microwavejournal.com/articles/10619-vector-receiver-load-pull-measurements`, [Accessed: Apr. 2025].

[17] D. M. Pozar, *Microwave Engineering*, international adaptation, 4th ed. WILEY, 2012, ISBN: 9781119770619.

[18] M. Litchfield and T. Cappello, "The various angles of outphasing PAs: Competitiveness of outphasing in efficient linear PA applications", *IEEE Microwave Magazine*, vol. 20, no. 4, pp. 135–145, 2019. DOI: `10.1109/MMM.2019.2891383`.

[19] W. Gerhard and R. Knoechel, "Improved design of outphasing power amplifier combiners", in *2009 German Microwave Conference*, 2009, pp. 1–4. DOI: `10.1109/GEMIC.2009.4815869`.

[20] C. Liang and B. Razavi, "Transmitter linearization by beamforming", *IEEE Journal of Solid-State Circuits*, vol. 46, no. 9, pp. 1956–1969, 2011. DOI: `10.1109/JSSC.2011.2148530`.

[21] C. A. Balanis, *Antenna Theory: Analysis and Design*, 4th ed. WILEY, 2016, ISBN: 9781118642061.

[22] W. L. Stutzman and G. A. Thiele, *Antenna Theory and Design*, 3rd ed. WILEY, 2013, ISBN: 9780470576649.

[23] T. Reveyrand, S. Hernández, S. Mons, and E. Ngoya, "SOLT and SOLR calibration methods using a single multiport "thru" standard connection", in *2020 95th ARFTG Microwave Measurement Conference (ARFTG)*, 2020, pp. 1–4. DOI: 10.1109/ARFTG47271.2020.9241365.

[24] Qorvo, Inc. "QPA9501 high power amplifier datasheet". Accessed: 2025-05-07. (2023), [Online]. Available: https://www.qorvo.com/products/p/QPA9501.

[25] J. Kalde, V.-P. Kutinlahti, A. Lehtovuori, A. Aabloo, and V. Viikari, "Leveraging mutual coupling in antenna-amplifier systems for increased reconfigurability", *IEEE Journal of Microwaves*, vol. 5, no. 1, pp. 59–67, 2025. DOI: 10.1109/JMW.2024.3499317.

A

Appendix

A.1 Exploratory Designs

This section discusses the exploratory designs, as introduced in Section 3.3.2. Some motivation on why these antennas were not used is provided

An attempt to recreate the antenna proposed in the conference paper *Linear LINC transmitters using dual-polarized power-combining antennas* by D. Tresnawan *et al* was made. However, issues arose when trying to replicate the results presented in the paper. This might be due to differences between simulating in ADS Momentum and CST. Aperture-coupled feeds have the strong benefit of allowing different substrate thicknesses and dielectric constants for the patch and the microstrip line. This could result in lower back-radiation. Furthermore, the design would allow for a single element antenna. These two factors make an antenna design like the one in Tresnawan's conference paper advantageous for outphasing applications.

One issue that might arise using this type of antenna is the polarization miss-match due to the orthogonally polarized signals from the ports. This could be remedied by using an orthogonally polarized receive antenna as well. Another option could be to design the ports such that the antenna is excited with the same polarization for the two ports.

Another design that was tried was a single patch antenna with orthogonally polarized in-set feed-lines, shown in Fig. A.1. The idea was to use a square patch with the resonance frequency 5.4 GHz. However, this antenna design did not work due to matching issues. The issue was that whenever the antenna ports were well-matched to 50 Ω, the coupling coefficients between the ports were too high, above −1 dB. The opposite also occurred; whenever the coupling coefficients were at a lower level, the reflection coefficients were too high.

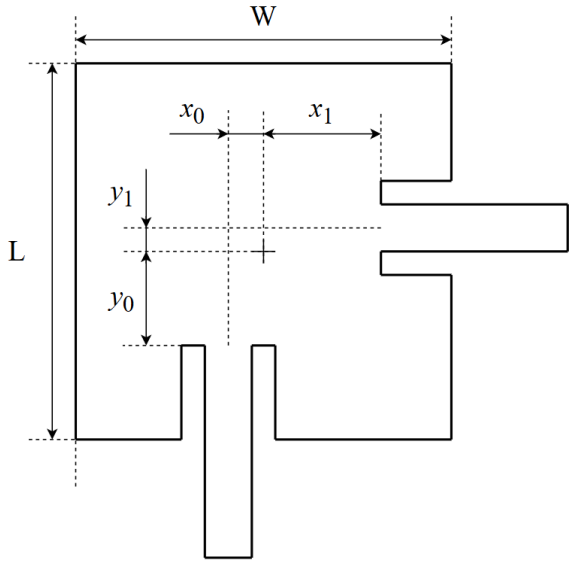

Figure A.1: Schematic of single patch antenna with two orthogonally polarized feed-lines.

A.2 CST Outphasing Simulation Data

This section presents the tables for the excitation-coefficients, accepted input power, IEEE gain and the non-normalized received power relevant to Section 4.4.

The CST outphasing data from both matching networks is presented in Table A.1 and Table A.2.

Table A.1: CST outphasing simulation results using lumped component matching network.

a_1 $[\sqrt{W}]$	a_2 $[\sqrt{W}]$	$P_{\mathbf{in}}$ [**W**]	$G_{\mathbf{IEEE}}$ [-]	$P_{\mathbf{r,\ non\text{-}normalized}}$ [**W**]
$2.35\underline{/0°}$	$2.30\underline{/0°}$	5.15	5.09	26.20
$2.29\underline{/15°}$	$2.32\underline{/-15°}$	5.12	3.93	20.13
$2.20\underline{/30°}$	$2.27\underline{/-30°}$	4.69	2.57	12.06
$2.09\underline{/45°}$	$2.18\underline{/-45°}$	4.10	1.26	5.14
$2.01\underline{/60°}$	$2.08\underline{/-60°}$	3.48	0.29	1.01
$1.97\underline{/75°}$	$1.98\underline{/-75°}$	3.05	0.02	0.05
$1.97\underline{/90°}$	$1.93\underline{/-90°}$	2.83	0.67	1.89
$2.02\underline{/105°}$	$1.91\underline{/-105°}$	2.86	3.28	9.36
$2.10\underline{/120°}$	$1.95\underline{/-120°}$	3.11	3.86	12.02
$2.20\underline{/135°}$	$2.02\underline{/-135°}$	3.59	5.24	18.80
$2.28\underline{/150°}$	$2.12\underline{/-150°}$	4.19	5.91	24.74
$2.34\underline{/165°}$	$2.22\underline{/-165°}$	4.78	5.81	27.80
$2.35\underline{/180°}$	$2.30\underline{/-180°}$	5.15	5.09	26.20

Table A.2: CST outphasing simulation results using microstrip matching network.

a_1 $[\sqrt{W}]$	a_2 $[\sqrt{W}]$	$P_{\mathbf{in}}$ **[W]**	$G_{\mathbf{IEEE}}$ **[-]**	$P_{\mathbf{r,\ non\text{-}normalized}}$ **[W]**
$2.11\underline{/0°}$	$2.09\underline{/0°}$	4.00	4.37	17.49
$2.21\underline{/15°}$	$2.02\underline{/-15°}$	4.09	3.13	12.81
$2.32\underline{/30°}$	$2.00\underline{/-30°}$	4.33	1.83	7.92
$2.39\underline{/45°}$	$2.04\underline{/-45°}$	4.58	0.74	3.37
$2.34\underline{/60°}$	$2.12\underline{/-60°}$	4.66	0.08	0.36
$2.26\underline{/75°}$	$2.19\underline{/-75°}$	4.66	0.22	1.00
$2.21\underline{/90°}$	$2.23\underline{/-90°}$	4.64	1.31	6.07
$2.18\underline{/105°}$	$2.28\underline{/-105°}$	4.67	3.03	14.14
$2.13\underline{/120°}$	$2.37\underline{/-120°}$	4.72	4.67	22.05
$2.05\underline{/135°}$	$2.38\underline{/-135°}$	4.56	5.65	25.79
$2.02\underline{/150°}$	$2.30\underline{/-150°}$	4.29	5.84	25.06
$2.04\underline{/165°}$	$2.19\underline{/-165°}$	4.07	5.35	21.78
$2.11\underline{/180°}$	$2.09\underline{/-180°}$	4.00	4.37	17.49

DEPARTMENT OF ELECTRICAL ENGINEERING
CHALMERS UNIVERSITY OF TECHNOLOGY
Gothenburg, Sweden
www.chalmers.se

CHALMERS
UNIVERSITY OF TECHNOLOGY